Santiago-Portillo, A.; Navalón Oltra, S.; Alvaro Rodríguez, MM.; García Gómez, H. (09-2). Generating and optimizing the catalytic activity in UiO-66 for aerobic oxidation of alkenes by post-synthetic exchange Ti atoms combined with ligand substitution. Journal of Catalysis. 365:450-463. https://doi.org/10.1016/j.jcat.2018.07.032

aGenerating and optimizing the catalytic activity in UiO-66 for aerobic oxidation of alkenes by post-synthetic exchange Ti atoms combined with ligand substitution

Andrea Santiago-Portillo, † Sergio Navalón, † Mercedes Álvaro, † Hermenegildo García*,†,§*

† Departamento de Química and Instituto de Tecnología Química CSIC-UPV, Universitat Politècnica de València, Av. de los Naranjos s/n, 46022 Valencia, Spain

§ Center of Excellence for Advanced Materials Research, King Abdulaziz University, Jeddah, Saudi Arabia

ABSTRACT. The catalytic activity for the aerobic epoxidation of cyclooctene of UiO-66 has been introduced by post-synthetic ion exchange of Zr^{4+} by Ti^{4+} at the nodes and the performance optimized by nitro substitution in the terephthalate ligand. In this way a TON value of 16,600 (1,660 considering Zr + Ti content) was achieved, comparing favorably with the highest catalytic activity reported in homogeneous for the same reaction (10,000 for γ-$SiW_{10}\{Fe^{3+}(OH_2)\}_2O_{38}^{6-}$). Kinetic studies have shown that the most likely reactive oxygen species involved in the oxidation is superoxide, with hydroxyl radicals also contributing to the reaction. UiO-66($Zr_{5.4}$ $Ti_{0.6}$)-NO_2 is stable under catalytic conditions, being used six times without any change in the conversion

temporal profile and in the X-ray diffractogram. The scope of UiO-66($Zr_{5.4}$ $Ti_{0.6}$)-NO_2 promoted aerobic oxidation of alkenes was expanded by including smaller rings cycloalkenes, as well as acyclic and aryl conjugated alkenes.

KEYWORDS. heterogeneous catalysis, aerobic oxidation of alkenes. metal-organic frameworks, UiO-66

1. INTRODUCTION

Transition metals have general catalytic activity to promote aerobic oxidations of hydrocarbons through different mechanisms, some of them involving reactive oxygen species.[1-3] While the use of oxygen as terminal oxidant, rather than peroxides or other oxidizing reagents, is very appealing due to availability, greenness and sustainability of the process, the lack of product selectivity limits, in most of the cases, the applicability of aerobic oxidations.[3-9]

Metal-organic frameworks (MOFs) are crystalline porous solids whose lattices are constituted by nodes of metal ions or clusters of metal ions, most frequently transitions metals, coordinated by rigid bi- or multidentate organic linkers.[10-13] Due to the high metal content, high surface area and high porosity, among other properties, MOFs are attracting much current interest as heterogeneous catalysts to promote organic reactions, including aerobic oxidations.[7, 14-23] As solid catalysts, MOFs offer various possibilities to introduce the catalytic activity by changing the nature of the metal ion[24-27] and also subsequent optimization by introducing substituents on the organic linker that are able to control the electronic density of the active metal sites by inductive effects.[28-30] Following the pioneer work of de Vos,[30] we and others[28, 29, 31-33] have shown that the activity of a given MOFs can be increased over one order of magnitude in Lewis or Brönsted acid catalyzed reactions[29] and some oxidations[28] by introducing electron withdrawing substituents on the aromatic ring of the terephthalate linker in MIL-101[28, 29, 31] and UiO-66.[30, 32, 33]

Continuing with this line of research aimed at exploiting the catalytic activity of MOFs, it would be of interest to create active sites in otherwise inactive MOFs by ion exchange at the nodes and, subsequently, optimization of their performance by substitution on the terephthalate linker.[34-36] In this regard, Li and coworkers have shown that it is possible to replace in UiO-66 (Zr) a certain

percentage up to about 30 % of Zr^{4+} metal ions by Ti^{4+} ions by post-synthetic modification of parent UiO-66(Zr) with $TiCl_4(THF)_2$ through ion exchange.[37] This strategy has been used, for instance, to increase the photocatalytic activity of parent UiO-66(Zr) for CO_2 reduction by introducing Ti^{4+} acting as electron relay between photoexcited terephthalate ligand and Zr^{4+}.[38]

To check this concept, and considering the known activity of Ti^{4+} grafted on mesoporous silicas and zeolites as oxidation catalysts, particularly in the presence of peroxides as oxidizing reagents, but also using oxygen as terminal oxidant,[39-45] in the present study we have focused on the reactivity of alkenes, particularly, cycloalkenes, to form the corresponding epoxide or allylic ol/one mixtures. The novelty of our study derives from the consideration that, as it will be described below, UiO-66(Zr) is devoid of any significant activity in the aerobic oxidation of cycloalkenes, but by applying known chemistry in the field of zeolites and aluminum silicates grafting Ti^{4+} it is possible to introduce active sites to promote this aerobic oxidation. Furthermore, it will be shown that the activity of UiO-66(Zr, Ti) can be increased by a factor of 8 when NO_2 is present on the terephthalate linker. In the area of Ti catalysts grafted on micro- and mesoporous materials, it was found that isolated titanium sites are active sites for epoxidation[43, 46, 47] and similar isolated Ti^{4+} sites can be easily obtained in UiO-66 by appropriate post-synthetic partial exchange Zr^{4+} by Ti^{4+} ion.

Although recent reports have confirmed incorporation of Ti in UiO-66 they have proposed that it occurs at defective sites where linkers are vacant through Ti attachment rather than ion exchanged.[48]

2. EXPERIMENTAL SECTION

2.1. Materials.

All the reagents and solvents used in this work were of analytical or HPLC grade and supplied by Merck.

2.2. Catalyst preparation.

Isoestructural UiO-66(Zr)-X (X: H, NO_2 and NH_2) were prepared following reported procedures.[32, 49-51] Briefly, the corresponding terephthalic acid derivative (1 mmol) and $ZrCl_4$ (1 mmol) were added to a Teflon-lined autoclave containing dimethylformamide (3 mL). The system was heated at the corresponding temperature for the required period of time (Table 1). After this time, the system was cooled down to room temperature and the resulting precipitate was first washed under stirring with DMF (40 mL) for 2 h (3 times) and, then, the solid was washed with methanol in a Soxhlet system for 12 h. Finally, the solid was dried in an oven at 100 ºC for 24 h.

Table 1. Temperature and time employed for the preparation of UiO-66-X (X: NH_2, H and NO_2) solids.[32]

X	Temperature (ºC)	Reaction time (h)
NH_2	100	24
H	220	12
NO_2	220	24

The three UiO-66-X (X: NH_2, H and NO_2) solids were further submitted to Zr^{4+} exchange using different percentages of Ti^{4+} following reported procedures.[49, 52] Briefly, UiO-66-X (X: NH_2, H and NO_2) solids (200 mg) were suspended in anhydrous DMF (5 mL) and magnetically stirred for 96 h at 120 ºC with freshly prepared $TiCl_4(THF)_2$ complex. $TiCl_4(THF)_2$ is prepared

immediately prior to its use by mixing $TiCl_4$ (2.9 mL) in anhydrous dichloroethane (50 mL) with 8.6 mL of THF in 100 mL of anhydrous *n*-hexane.

2.3. Catalyst characterization.

Powder X-ray diffraction (PXRD) patterns of UiO-66(Zr Ti)-X (X: NH_2, H and NO_2) materials were recorded on a Philips XPert diffractometer equipped with a graphite monochromator (40 kV and 45 mA) employing Ni filtered Cu Kα radiation. ATR-FTIR spectra of UiO-66(Zr,Ti)-X materials were collected at 20 ºC using a Bruker Tensor27 instrument. Previously, the solid samples were heated in an oven (100 ºC for 20 h) to remove physisorbed water. N_2 adsorption isotherms were recorded at 77 K using a Micromeritics ASAP 2010 instrument. Thermogravimetric measurements were performed on a TGA/SDTA851e Mettler Toledo station. Scanning electron microscopy (SEM, Zeiss instrument, AURIGA Compact) having incorporated a EDX detector has been employed to determine the morphology of the solid samples and obtain the element mapping of selected areas, respectively. The EDX detector has a limit of detection of about 1 wt%. X-ray photoelectron (XP) spectra were collected on a SPECS spectrometer with a MCD-9 detector using a monochromatic Al (Kα= 1486.6 eV) X-ray source. Spectra deconvolution was performed with the CASA software using the C 1s peak at 284.4 eV as binding energy reference.[53]

The metal content (Zr and/or Ti) of solid samples have been determined by ICP-OES analysis. Previously, the solid samples (5 mg) were digested using a HNO_3 aqueous solution (3 M, 30 mL) at 80 ºC for 12 h. Then, the filtered aqueous samples were analyzed by ICP-OES.[37]

FTIR spectra of CO adsorption were recorded in a Nexus 8700 FTIR spectrophotometer using an IR cell allowing *in situ* treatments at controlled temperature, from -176 ºC to 500 ºC, and

connected to a high vacuum system with gas dosing facility. For CO adsorption measurements the samples were pressed into self-supported wafers and treated under vacuum (10^{-6} mbar) at 150 ºC for 2 h. After activation, the wafers were cooled down to -176 ºC under dynamic vacuum, followed by CO dosing at increasing pressure (0.4-6 mbar). IR spectra were collected after each dosage. All IR spectra corresponding to CO adsorption measurement have been normalized to the weight of the IR wafer.

Catalytic experiments.

Briefly, the required amount of UiO-66(Zr Ti)-X (X: NH_2, H and NO_2) employed as catalyst (0.016 mmol of total metal Zr+Ti) was introduced into a reactor vessel (5 mL). Subsequently, the olefin reagent (2 mmol) dissolved in CH_3CN (2.5 mL) was added to the vessel. The system was pressurized with O_2 at the required value at room temperature (i.e. 5 or 2 atm). The reactions were carried out under 600 rpm magnetic stirring to ensure that the process is under kinetic control.

Catalyst reusability was studied for the most active sample (UiO-66($Zr_{5.4}Ti_{0.6}$)-NO_2). At the end of the reaction, the solid catalyst was recovered by filtration (Nylon membrane, 0.2 μm) and, transferred to a round-bottom flask (50 mL) and washed under magnetic stirring with ethanol (20 mL) at 80 ºC for 2 h. This procedure was repeated three times. The washed, used solid catalyst was recovered by filtration (Nylon membrane, 0.2 μm) and dried in an oven at 100 ºC for 24 h. Before the new catalytic cycle, the solid catalyst was activated at 150 ºC under vacuum for 16 h.

Selective radical quenching experiments were carried out following the general reaction procedure described above, but with the addition of radical quenchers (20 mol% with respect to the substrate). In particular, dimethylsulfoxide (DMSO) [54-57] or *p*-benzoquinone [54, 55, 57, 58] were added as selective hydroxyl or superoxide/hydroperoxyl radical scavengers, respectively.

Activation energy for cyclooctene was estimated according the Arrhenius law by plotting the natural logarithm of the initial reaction rate of cyclooctene disappearance versus the reciprocal of the absolute temperature, fitting the experimental points to the best linear correlation. The amount of oxygen consumed was estimated from the difference of the reactor pressure before and after the reaction.

Product analysis.

Previously filtered reaction aliquots were diluted in acetonitrile containing a known amount of nitrobenzene as external standard. The aliquots were immediately analyzed by gas chromatography using a flame ionization detector. Quantification was carried out by using calibration curves of authentic samples against nitrobenzene as standard. Mass balances for all the reactions were higher than 95%. Product yields can be estimated by multiplying conversion by selectivity.

Leaching experiments.

At the end of the reaction the solid was removed by filtration (0.2 μm nylon filter) and the solvent removed under vacuum in a rotary evaporator. Then, an aqueous solution of HNO_3 (3 M, 30 mL) was added to the flask reaction and the system heated at 80 ºC for 24 h. Finally, the presence of Zr or Ti in the aqueous phase was analyzed by ICP-OES.

Colorimetric peroxide quantification of treated UiO-66 ($Zr_{5.4}Ti_{0.6}$)-H

Prior to peroxide titrations, an acidic aqueous solution (100 mL) of titanyl oxalate (2.5 g) in $H_2SO_{4(c)}$ (25 mL) and $HNO_{3(c)}$ (1 mL) was prepared. Then, 10 mg of UiO-66 ($Zr_{5.4}Ti_{0.6}$)-H was heated at 120 ºC under 5 atm oxygen pressure in 2 mL of acetonitrile for 24 hours. After this time,

the solid was dissolved in the acidic titanyl solution where $Ti{=}O^{2+}$ acts as peroxide colorimetric indicator.[59] An aliquot sample (0.5 mL) was diluted with water (4.5 mL) before measuring its absorbance at 420 nm. The difference in absorbance between this sample and an analogous one that was not submitted to 24 hours treatment was compared. Formation of peroxide was not detected.

EPR measurements.

UiO-66($Zr_{5.4}$ $Ti_{0.6}$)-NO_2 or UiO-66(Zr)-NO_2 (5 mg) was added to a two-neck round bottom flask (25 mL) containing the commercially available spin trap N-*tert*-butyl-α-phenylnitrone (PBN, 1150 mg L^{-1}) dissolved in n-dodecane. The system was sonicated for 30 min and purged with a balloon containing O_2. Then, the flask is heated at 120 ºC for 6 h. At this time, a reaction aliquot is filtered (Nylon filter, 0.2 μm) and the sample was purged with N_2 before recording the EPR. EPR spectrum of each sample was acquired using a Bruker EMX instrument operating at a frequency of 9.803 GHz with sweep width of 3489.9 G, a time constant of 40.95 ms, a modulation frequency of 100 kHz, a modulation width of 1 G and a microwave power of 19.92 mW.

3. RESULTS AND DISCUSSION

3.1. Catalyst characterization

The list of catalyst prepared in the present study, the most relevant textural properties and analytical data are summarized in Table 2. As it can be seen there, three sets of isostructural UiO-66 having on the terephthalate linker a nitro or amino substituents, as well as the parent terephthalate were prepared at four different levels of Zr^{4+} by Ti^{4+} ion exchange. Preparation of isostructural UiO-66-H, UiO-66-NO_2, UiO-66-NH_2 was carried out as

reported in the literature.[32, 49] Briefly, the three UiO-66(Zr) were prepared by solvatothermal crystallization of $ZrCl_4$ and terephthalic, 2-nitroterephthalic and 2-aminoterephthalic ligand in DMF. The conditions and the exact mass of the components are indicated in Table 1 of the experimental section. The three UiO-66-X (X:H, NO_2, NH_2) were further submitted to Zr^{4+} to Ti^{4+} exchange in DMF at 120 ºC by increasing the concentration of $TiCl_4(THF)_2$ complex to afford for each case of linker substituted UiO-66-X new mixed-metal materials with increasing Ti content ranging for 0 to 10 %.[49, 52]

Since Zr^{4+} ion forms with carboxylate a strong coordinative bond, it has been found that is not possible to achieve a high level of exchange. In the present case,[60] the maximum Zr^{4+} to Ti^{4+} exchange level achieved was 10%. It has been proposed that Ti^{4+} exchange in UiO-66(Zr) occurs due to the intrinsic dynamics around the Zr^{4+} ions that can change the instantaneous coordination number.[61] Precedents reporting Ti^{4+} exchanged in UiO-66 to improve the performance of this MOF for gas permeability[62] or in photocatalysis can be found in the literature.[22, 48]

Table 2. List of catalysts employed in the present study with their corresponding BET surface area, pore volume, metal content and initial reaction rate for the catalytic aerobic epoxidation of cyclooctene.[a]

Catalyst	BET Surface Area (m^2 g^{-1})	Pore Volume (cm^3 g^{-1})	ICP Zr (%)	ICP Ti (%)	r_0 (mM h^{-1})
UiO-66(Zr)-NO_2	600	0.60	100.00	-	2.02
UiO-66($Zr_{5.97}$ $Ti_{0.03}$)-NO_2	520	0.46	99.49	0.51	6.34
UiO-66($Zr_{5.94}$ $Ti_{0.06}$)-NO_2	580	0.52	98.40	1.60	7.01
UiO-66($Zr_{5.4}$ $Ti_{0.6}$)-NO_2	590	0.50	89.60	10.40	9.83
UiO-66(Zr)-H	800	0.75	100.00	-	1.25
UiO-66($Zr_{5.97}$ $Ti_{0.03}$)-H	770	0.78	99.42	0.58	3.83
UiO-66($Zr_{5.94}$ $Ti_{0.06}$)-H	740	0.68	98.80	1.20	4.98
UiO-66($Zr_{5.4}$ $Ti_{0.6}$)-H	740	0.77	89.40	10.60	6.94
UiO-66(Zr)-NH_2	780	0.85	100.00	-	1.20
UiO-66($Zr_{5.97}$ $Ti_{0.03}$)-NH_2	720	0.50	99.40	0.60	2.38
UiO-66($Zr_{5.94}$ $Ti_{0.06}$)-NH_2	730	0.52	98.50	1.50	3.97
UiO-66($Zr_{5.4}$ $Ti_{0.6}$)-NH_2	770	0.51	89.60	10.40	6.09

[a] Catalyst (0.016 mmol of metal), substrate (2 mmol), CH_3CN (2 mL), 120 ºC and O_2 (5 atm).

As it can be seen in Figure 1 and Figures S1-S2, PXRD of all the UiO-66-X (Zr_{6-x} Ti_x) samples exhibited identical pattern corresponding to a highly crystalline material. As expected in view of the reported data, the presence of Ti^{4+} in the material causes a gradual shift of the most intense (111) peak from the initial 2θ value at 7.39 º to higher diffraction angles reaching 2θ values of 7.43 º. This effect of gradual shift in the position of the diffraction peaks has been previously reported in the literature and has been rationalized as a reflection of the somewhat smaller unit cell of UiO-66($Zr_{6-x}Ti_x$) due to the contraction caused by the smaller ionic radius of Ti^{4+} compared to Zr^{4+}.[37, 52] Therefore, according to the literature the gradual shift of the position of (100) diffraction peak observed for each series of UiO-66(Zr Ti)-X (X: H, NO_2 or NH_2) is considered here an evidence of substitution of Zr^{4+} by Ti^{4+} in the lattice.[37, 52]

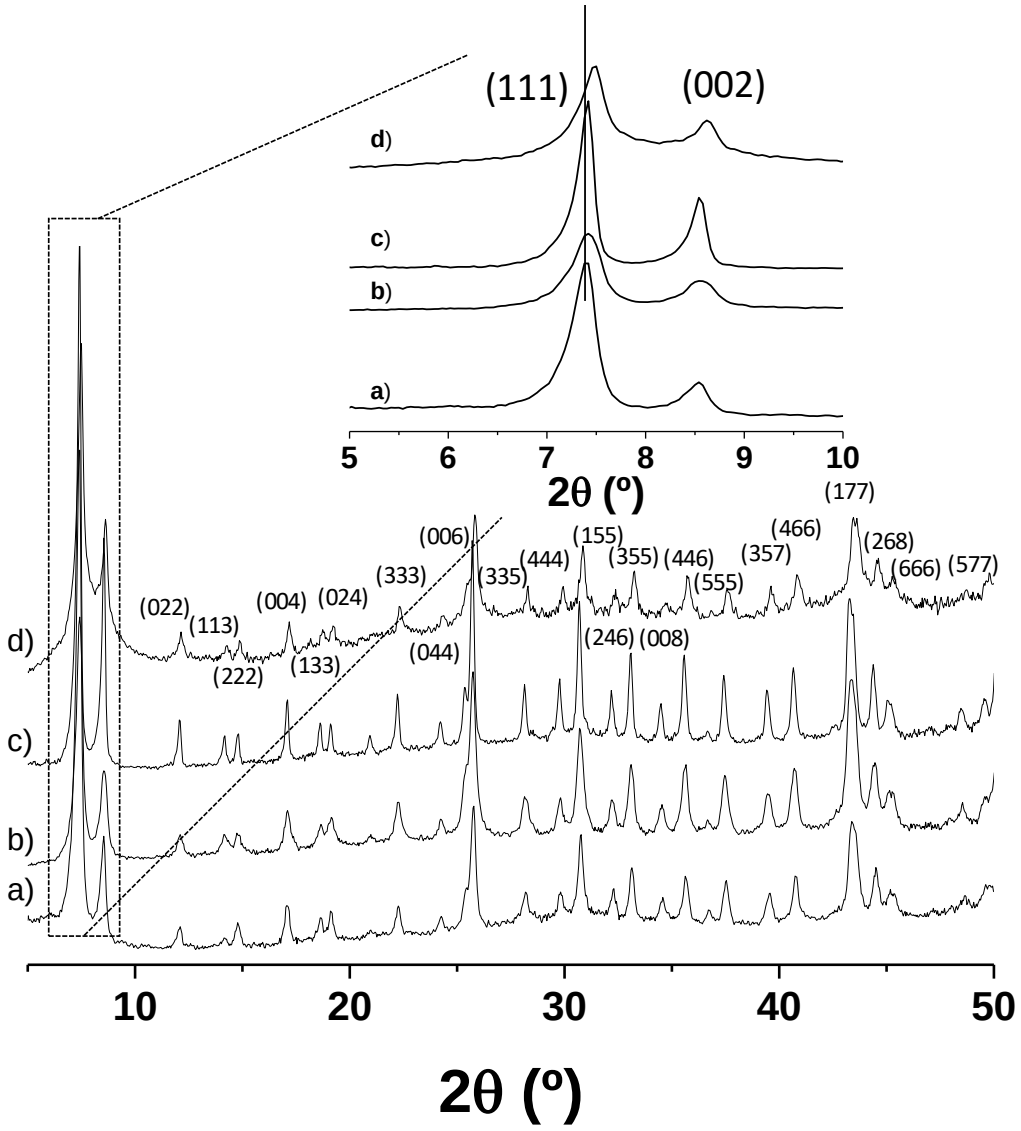

Figure 1. PXRD patterns of UiO-66(Zr)-H (a), UiO-66($Zr_{5.97}$ $Ti_{0.03}$)-H (b), UiO-66($Zr_{5.94}$ $Ti_{0.06}$)-H (c), UiO-66($Zr_{5.4}$ $Ti_{0.6}$)-H (d).

The different substitution of the terephthalate linker is confirmed by IR spectroscopy of the solids, where the characteristic vibrational peaks associated to NO_2 (1500 and 1380 cm^{-1}) and NH_2 (3350 and 1595 cm^{-1}) can be observed (Figures S3-S5). In contrast, the partial substitution of Zr^{4+} by Ti^{4+} ions in the UiO-66(Zr)-NO_2 materials does not cause significant changes in their FT-IR spectra (Figure S4).

Isothermal nitrogen adsorption measurements indicate that the specific surface area and pore volumes of the UiO-66-X samples under study range from 890 to 520 m^2 g^{-1} and 0.46 to 0.85 cm^3 g^{-1}, respectively (Table 2). These values and the general trend observed, where the surface area of each parent UiO-66-X (X: H, NO_2 or NH_2) based material, although similar, decreases along the extent of the ion exchange, is in agreement with previous reports.[27, 52]

Thermogravimetry under aerobic conditions offers important information related to the presence of defects in the material, by comparing the experimental residual weight after complete combustion on the organic linker that is assumed to correspond to $Zr_{6-x}Ti_xO_2$ residue with the theoretical weight of the residue calculated based on the structural formula.[28, 29] Thermogravimetric profiles (Figures S6-S8) exhibit an initial weight loss from room temperature to 150 ºC that corresponds to the desorption of co-adsorbed water and solvent molecules. After this step, there is an exothermic weight loss attributable to the combustion of the organic linker that takes places in all the samples under study from 250 to 400 ºC. The difference between the experimental residual weight in the thermogravimetric profile at 800 ºC with that calculated based on the molecular formula, either positive and negative, indicates that excess or defective amount of metal oxides in the material respect to the ideal value according to the formula. In the present case, the excessive weight of the residue in the TGA indicates either an excess of Zr/Ti in the material or vacancies of terephthalate linkers in the solid as indicated in Table S1. It is known in the state of the art that UiO-66(Zr) can present a large density of defects that can be quantified in a simple way by the difference between the theoretical an experimental chemical analysis.[63] It should be mentioned that the experimental error associated to thermogravimetric measurements does not allow to determine differences in the residual weight for those samples with the lowest Ti exchange percentage. A summary of the relevant experimental thermogravimetric data and its

comparison with the theoretical value is presented in Table S1. As it can be seen there, the parent UiO-66(Zr)-X (X: H, NO_2 or NH_2) before Ti exchange treatments exhibit somewhat higher (~ 1 wt%) percentages of Zr than calculated according to the ideal cell formula that range from 0.3 for UiO-66(Zr)-NH_2 to 0.9 % for UiO-66(Zr)-NO_2, indicating that the materials contain some defects associated to a larger than ideal amount of Zr. Those defects can be, for instance, terephthalate vacancies or the presence of amorphous zirconium oxide clusters in the material. To put into context the data presented in Table S1 showing just a relatively minor higher-than-expected Zr content, the density of defects in our case should be relatively low in comparison with other precedents reported in the literature, where Zr excess higher than 10 % have been determined.[32, 64] Upon submitting UiO-66(Zr)-X to Ti exchange in the largest proportion (10 %), a change in the residual remaining weight in the material due to the lower atomic mass of Ti (47.9 a.u.) respect to Zr (91.2 a.u.) should be expected according to the cell formula. Specifically, the decrease in the residual weight due to the Zr to Ti exchange should theoretically be between 2.4 wt% in the case of UiO-66($Zr_{5.4}$ $Ti_{0.6}$)-NO_2 to 2.8 wt% for UiO-66($Zr_{5.4}$ $Ti_{0.6}$)-H. Importantly this decrease in the percentage of the residual weight of less than 3 % in the residual mass measured was experimentally observed by TG. Experimental measurements of the decrease of residue mass range between -1.9 and -2.3 % for UiO-66(Zr)-NO_2 and UiO-66(Zr)-NH_2, respectively, as indicated in Table S1. These analytical data are in agreement with the exchange of a heavier metal element as Zr by another lighter as Ti in measurable degree.

XPS analysis of UiO-66(Zr/Ti)-X (X: H, NO_2 or NH_2) also detects the presence of titanium for those samples submitted to Ti exchange. In the particular case of the UiO-66(Zr Ti)-NO_2 series the Ti/Zr atomic ratio increases in all cases with the percentage of the ion exchanged and it was always higher than the values determined by other analytical methods (Figure 2a). This is probably

due to the fact that XPS is a surface specific technique and, therefore, there should probably be a gradient of titanium content that should be higher on the external surface of the MOF particles, decreasing this Ti/Zr ratio towards the interior of the UiO-66-NO_2 crystallites. Figure 2a shows the survey XPS spectra revealing the presence of the different elements in the UiO-66(Zr)-NO_2 material, as well as in the partially substituted UiO-66($Zr_{6-x}Ti_x$)-NO_2 solids (Figures S9-S12). As expected the Ti/Zr atomic ratio increases in all cases with the percentage of the ion exchanged, in agreement with the successful incorporation of Ti^{4+} in the solid material. Figure 2b-d also shows a shift in the binding energies of Zr 3d, Ti 2p and O 1s peaks as the Ti^{4+} content increases. There are precedents in the literature suggesting that these shifts in XPS binding energy reflect the weaker electronegativity probed by the metallic elements as the Zr^{4+} ions are partially exchanged by Ti^{4+}, and the same explanation should apply in the present case.[27, 49, 65-67]

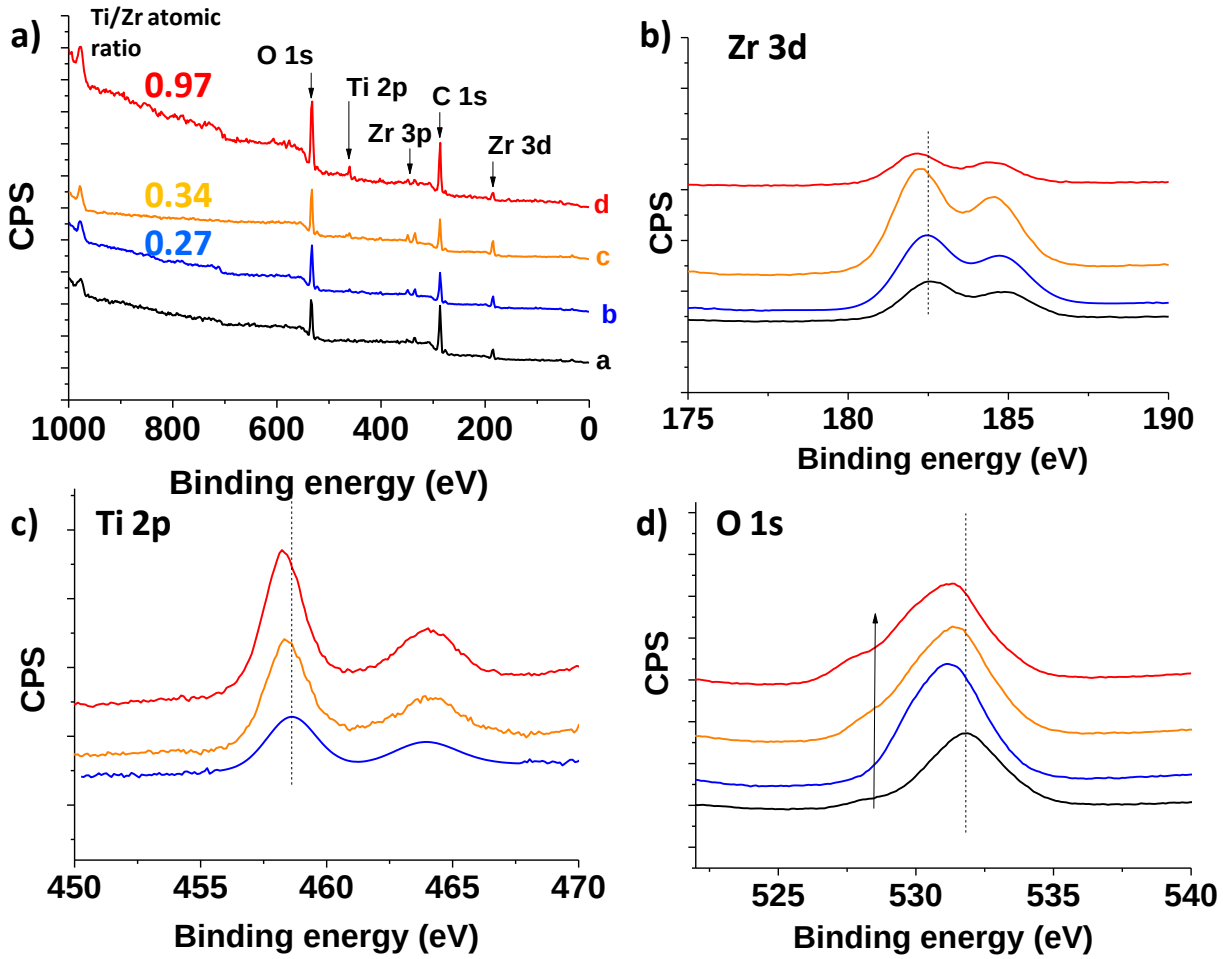

Figure 2.: XPS spectra of survey (a) and the high resolution scan of Zr 3d (b), Ti 2p (c) and O 1s (d) regions for the UiO-66(Zr6-xTix)-H sample.

Diffuse reflectance UV-Vis spectra for the series of the UiO-66 materials were recorded (Figure 3 and Figures S13-S14). As it can be reported[27, 32] it was generally observed a red shift on the absorption on set, the partial substitution of Zr^{4+} ions by Ti^{4+} results in extending the absorption of the parent UiO-66(Zr)-X (X: H, NO_2 or NH_2) material at longer wavelengths.[27, 52]

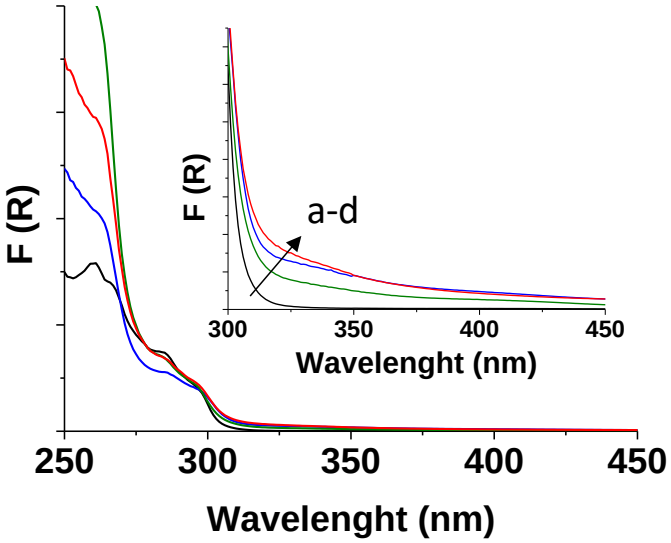

Figure 3. Diffuse reflectance UV-Vis of UiO-66(Zr)-H (a), UiO-66($Zr_{5.97}$ $Ti_{0.03}$)-H (b), UiO-66($Zr_{5.94}$ $Ti_{0.06}$)-H (c) and UiO-66($Zr_{5.4}$ $Ti_{0.6}$)-H (d).

The morphology of the UiO-66(Zr)-X particles was visualized by SEM (Figure 4 and Tables S2-S4). SEM images of the UiO-66(Zr)-X samples before Ti exchange show that the material is constituted by crystals with defined shape in the micrometric scale, accompanied by much smaller nanometric particles. EDS mapping of the individual particles shows the homogeneous distribution of the elements according to their cell formula. Importantly, the morphology of the particles changes somewhat during the ion exchange procedure, the change being characterized by a decrease in the population of large crystals and a concomitant increase in the percentage of much smaller nanometric particles. This morphology change suggests that there is some breakdown of large particles during the ion exchange. Elemental mapping at submicrometric resolution by EDS shows that Ti is homogeneously distributed in the particle (Figure 4 and Figures S15-S25). Particularly at large percentages of Ti exchange for which the Ti Kα1 images are better defined, a coincidence the distribution of Zr and Ti can be observed, confirming that Ti is present at the same positions as Zr at submicrometric resolution. Figure 4 shows selected images to illustrate these

two pieces of information provided by SEM, i.e., the increase in the percentage of smaller particles with the increase in the percentage of Ti and the coincidence between the distribution of Zr and Ti in the individual particles.

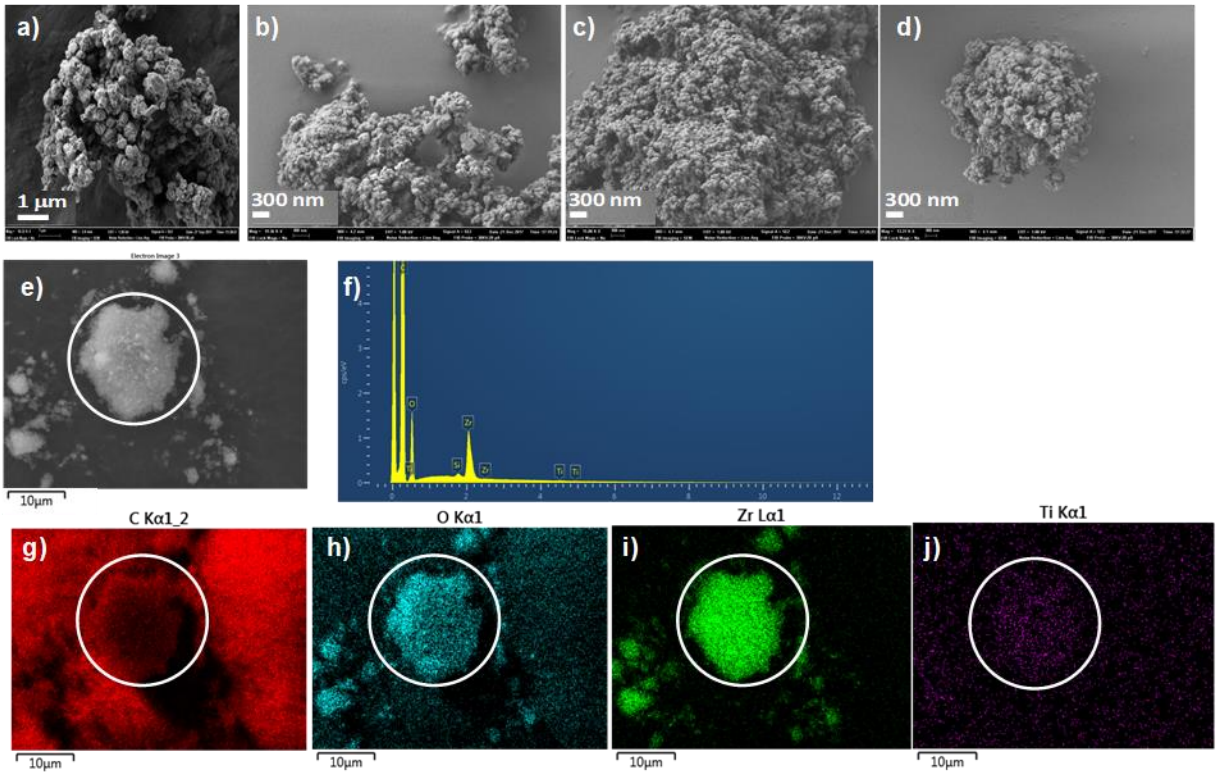

Figure 4. SEM images of UiO-66(Zr)-H (a), UiO-66($Zr_{5.97}$ $Ti_{0.03}$)-H (b), UiO-66($Zr_{5.94}$ $Ti_{0.06}$)-H (c) and UiO-66($Zr_{5.4}$ $Ti_{0.6}$)-H (d). Mapping and spectrum of selected image of UiO-66($Zr_{5.94}$ $Ti_{0.06}$)-H (e-j).

3.2. CATALYTIC ACTIVITY

As commented earlier, evaluation of the catalytic activity of UiO-66(Zr,Ti)-X samples was initially carried out for the aerobic oxidation of cyclooctene in CH_3CN. The only product observed in all cases was the corresponding cyclooctene oxide with complete selectivity (Figure 5a) and complete mass balance. It was observed that the presence of UiO-66 (0.8 mol%) does not introduce any significant catalytic activity respect to the blank control (Figures 6, S26 and S27). In contrast, it was observed that the catalytic activity for the series of materials with the three differently substituted terephthalates increases consistently with the percentage of the Ti exchange and it is higher for the NO_2 (Figure 5), then for H (Figure S26) and the NH_2 (Figure S27) terephthalate substituted UiO-66 series, being UiO-66(Zr)-NH_2 the less active of the samples under evaluation. The performance of the series of UiO-66(Zr Ti)-X can be quantitatively evaluated by comparing the initial reaction rates, determined from the slope of the time-conversion plots at zero time. These values are summarized in Table 2.

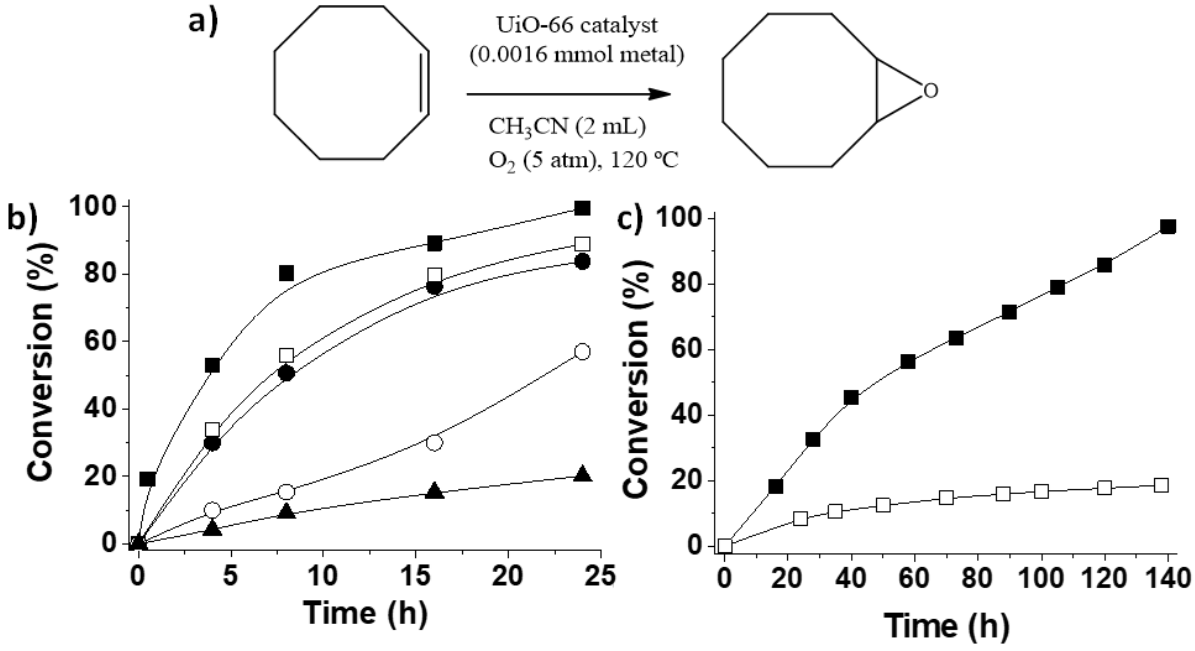

Figure 5. a) Aerobic oxidation of cyclooctene by UiO-66 based catalysts; b) Time–conversion plot for the aerobic oxidation of cyclooctene to cyclooctene oxide using UiO-66-NO_2 as catalyst. Legend: UiO-66($Zr_{5.4}$ $Ti_{0.6}$)-NO_2 (■), UiO-66($Zr_{5.94}$ $Ti_{0.06}$)-NO_2 (□), UiO-66($Zr_{5.97}$ $Ti_{0.03}$)- NO_2 (●) UiO-66(Zr)-NO_2 (○) and blank control in the absence of catalyst (▲). Reactions conditions: Catalyst (0.016 mmol of metal), substrate (2 mmol), CH_3CN (2 mL), 120 ºC and O_2 (5 atm). c) Time–conversion plot for the aerobic oxidation of cyclooctene to cyclooctene oxide under productivity test conditions using a low amount of UiO-66($Zr_{5.4}$ $Ti_{0.6}$)-NO_2. Legend: UiO-66($Zr_{5.4}$ $Ti_{0.6}$)-NO_2 (■) and blank control in the absence of catalyst (□). Reaction conditions: Catalyst (0.006 mmol of metal), substrate (10 mmol), CH_3CN (3 mL), 120 ºC and O_2 (5 atm).

Therefore, according to this table, the most active material was UiO-66($Zr_{5.4}$ $Ti_{0.6}$)-NO_2 in where the beneficial influence of the presence of Ti ions introducing active sites and nitro substituents optimizing the performance are combined. Regarding the active sites and the role of Ti^{4+}, it should be noted that, as clearly seen in Figure S26 and S27, the catalytic activity of UiO-66(Zr)-H and UiO-66(Zr)-NH_2 is coincident with that of a blank control in the absence of any solid. This indicates that in the absence of Ti, UiO-66(Zr)-H and UiO-66(Zr)-NH_2 do not exhibit any catalytic activity. Accordingly, it is proposed that Ti^{4+} are the active sites in this aerobic oxidation. Furthermore, as it can be seen in Table 2 and Figures 6, S26 and S27, the initial reaction rate increases almost linearly with the Ti content, up to a certain Ti/Zr exchange value beyond with the increase in the initial reaction rate is less important reinforcing the proposal that this metal is the site promoting oxidation (Figure S28). Since according to Table S1, the density of defects, although low, also increases with the percentage of Ti exchange, the possibility that the defects created in the process of Ti^{4+} exchange are the real sites, rather than the Ti^{4+} ions or associated

with it, cannot be disregarded with the present catalytic data. However, if defects of other nature unrelated to the presence of Ti^{4+} were responsible for the catalytic activity, no direct relationship between the catalytic activity and the percentage of Ti^{4+} should be expected. Therefore, the present kinetic data rather supports the role of Ti^{4+} as active sites.

Using the most active UiO-66($Zr_{5.4}Ti_{0.6}$)-NO_2 material a productivity test was performed as well as the sample was submitted to consecutive reuses. The purpose is to determine the stability of UiO-66($Zr_{5.4}$ $Ti_{0.6}$)-NO_2 under catalytic conditions, by using, in one case, a large excess of substrate with respect to the amount of catalyst (productivity test) and, in the other, to establish the variation of the temporal evolution upon consecutive reuses. For the productivity test (Figure 5b) complete cyclooctene conversion with complete selectivity toward cyclooctene oxide was achieved in 6 days. In this way a turnover number (TON) of 1,660 considering the total amount of metal as the active site, or 16,600 if only the titanium content is considered was estimated. This TON value as well as the TOF (6,640 h^{-1} at 20% conversion) compares favorably with other reports in homogeneous aerobic oxidation using heteropolyacids (TON 10,000 and TOF 22 h^{-1} at 20 % conversion for γ-$SiW_{10}\{Fe^{3+}(OH_2)\}_2O_{38}^{6-}$; reaction conditions: catalyst 1.5μmol, solvent 1,2-dichloroethane/acetonitrile 1.5/0.1 mL, substrate 18.5 mmol, O_2 1 atm).[68] And even though others in heterogeneous catalysis that oxidize cycloalkenes by H_2O_2 employing CH_3ReO_3 (TON 20,000 and TOF 666 h^{-1} at 20 % conversion; reaction conditions: 0.001 mmol CH_3ReO_3, 20 mmol cyclooctene, 40 mmol H_2O_2, 2 mmol 3-methylpyrazole in 10 mL CH_2Cl_2)[69] and Ta_2O_5/SiO_2 (TON 150 and TOF 720 h^{-1} at 40 % of conversion; reaction conditions: 30 mg of catalyst, 6 mL CH_3CN, 300 μL DCB, 0.77M cyclooctene, 0.51 M H_2O_2, 60 ºC).[70]

It should be noted however that comparison of the absolute catalytic activity from literature data is always not fear due to the different temperature and conditions employed in the oxidations.

Very similar temporal profiles for cyclooctene disappearance were observed for six consecutive reuses of UiO-66($Zr_{5.4}$ $Ti_{0.6}$)-NO_2 (Figure 6). The minor changes in the initial reaction rates in the recycling test are probably due to the incomplete recovery of the solid in the filtration of the catalyst after the reaction. To confirm the stability of UiO-66($Zr_{5.4}$ $Ti_{0.6}$)-NO_2 chemical analysis of the liquid phase was carried out to determine the absence of Zr and Ti, experimental data indicating that the amount of Zr and Ti leached is less than 0.5%. Moreover, crystallinity of UiO-66($Zr_{5.4}$ $Ti_{0.6}$)-NO_2 after its use as catalyst was confirmed by recording PXRD pattern upon reuse, whereby no significant changes in the crystallinity of the material were observed. Therefore, all the available data, the very low Zr^{4+} and Ti^{4+} leaching, coincidence of the temporal profiles upon reuse, lack of variation of PXRD patterns, indicate the stability of the material under the reaction conditions.

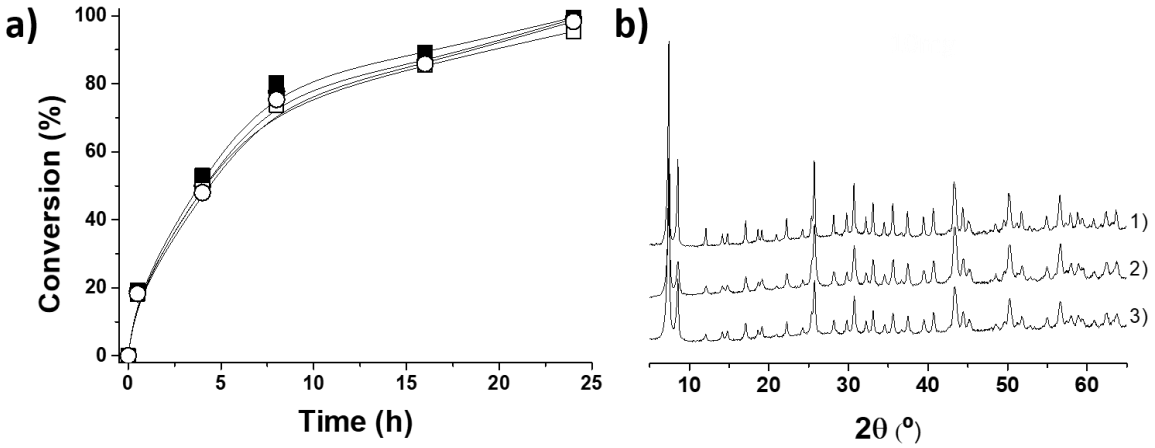

Figure 6. a) Reusability experiments employing UiO-66($Zr_{5.4}$ $Ti_{0.6}$)-NO_2 as catalyst in the aerobic oxidation of cyclooctene to cyclooctene oxide. Legend: 1st use (■), 2nd use (□), 4th use (●) and 6th use (○). b) PXRD of fresh UiO-66($Zr_{5.4}$ $Ti_{0.6}$)-NO_2 (1), three times used UiO-66($Zr_{5.4}$ $Ti_{0.6}$)-NO_2 (2) and six times used UiO-66($Zr_{5.4}$ $Ti_{0.6}$)-NO_2 (3). Reactions conditions: Catalyst (0.016 mmol of metal), substrate (2 mmol), CH_3CN (2 mL), 120 ºC and O_2 (5 atm).

Additional control experiments were performed using 2-nitroterephthalic acid as promoter or ZrO_2 or TiO_2 at the percentage contained in UiO-66(Zr Ti)-NO_2 or just the amount measured by leaching. In particular, the presence of 2-nitroterephtalic acid has not any activity to promote cyclooctene epoxidation. The results are presented in Figure 7 that shows that the catalytic activity of UiO-66(Zr Ti)-NO_2 is much higher in terms of initial reaction rate or final conversion than any of these five controls. Besides, the catalytic of mixed-metal UiO-66(Zr Ti)-NO_2 was also notably much higher than that of MIL-125(Ti), showing the benefits of large porosity and Ti distribution of UiO-66(Zr Ti)-NO_2 respect to MIL-125(Ti). Comparison of the performance of UiO-66(Zr Ti)-NO_2 and MIL-125(Ti) illustrates the importance of Ti site isolation at the $Zr_5Ti(O)_4(OH)_4$ nodes and the large cavities of UiO-66.

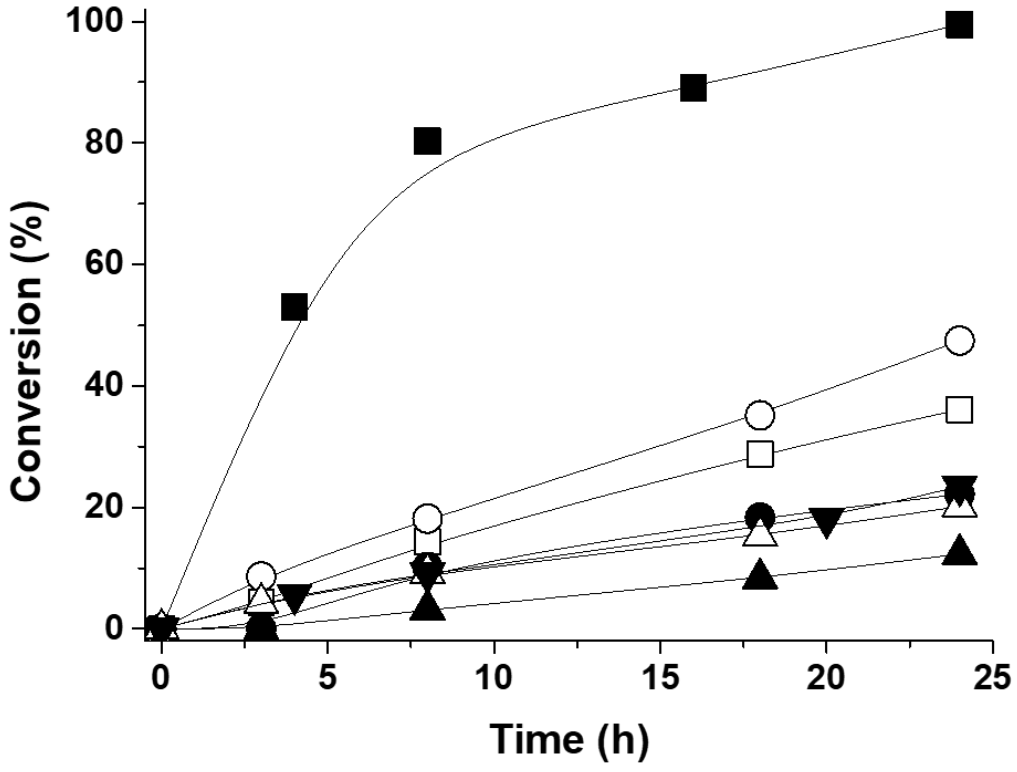

Figure 7. Time–conversion plots for the aerobic oxidation of cyclooctene to cyclooctene oxide using different catalysts. Legend: UiO-66($Zr_{5.4}$, $Ti_{0.6}$)-NO_2 (■), MIL-125 (Ti) (□), ZrO_2 (●) TiO_2 (○) ZrO_2 with the amount of metal leached (▲), TiO_2 with the amount of metal leached (Δ) and 2-nitroterephthalic acid with the amount of ligand that in MOF (▼). Reactions conditions: Catalyst (0.016 mmol of metal), substrate (2 mmol), CH_3CN (2 mL), 120 ºC and O_2 (5 atm).

To understand the role of UiO-66(Zr Ti)-X as catalyst in this aerobic oxidation, as well as to determine the heterogeneity of the catalysis, a hot filtration test in which the temporal profile of two twin reactions, one of them in the presence of the catalyst and the other initiated with the solid catalyst and, then, removing the solid at the reaction temperature and the resulting clear solution allowed to continue the reaction in the absence of solid were compared. The results obtained are presented in Figure 8. As it can be seen there, in one of the two parallel reactions the catalyst was filtered at 0.5 h reaction time, when cyclooctene conversion was about 20 %. Comparison of the two time-conversion plots shows that, although the reaction in the absence of catalyst progressed about 50 % less than in the presence of the solid catalyst, there is a substantial cyclooctene to cyclooctene oxide conversion in the clear solution after removal of the catalyst. It is worth to comment that according to Figure 5, under the reaction conditions, some autooxidation of cyclooctene (about 30 %) occurs in the absence of any catalyst. However, in the present case, after filtration of the catalyst, the conversion of cyclooctene increases from 20 to 50 % that is significantly higher than the non-catalytic conversion expected according to the blank reaction (about 20 % for the same reaction time, Figure 5). Overall, the catalytic data indicate that after initiation of the oxidation by UiO-66($Zr_{5.4}$ $Ti_{0.6}$)-NO_2 some reactive oxygen species or leached

species or reaction intermediates present in the liquid phase may contribute somewhat (~ 30 %) to the overall conversion observed for the catalytic experiment without removal of the solid.

Possible species present in the liquid phase that could contribute to the progress of the reaction after removal of the catalyst include H_2O_2, organic hydroperoxides and peroxides as well as colloidal ZrO_x or TiO_x nanoparticles. Since the amount of O_2 consumed in the reaction, as determined from the decrease in the reactor pressure, is stoichiometric with cyclooctene conversion within the error limit (0.975 mmol), it can be inferred that the percentage of this oxygenated intermediates, including any possible reaction with the solvent, should be low, barely in the detection limit.

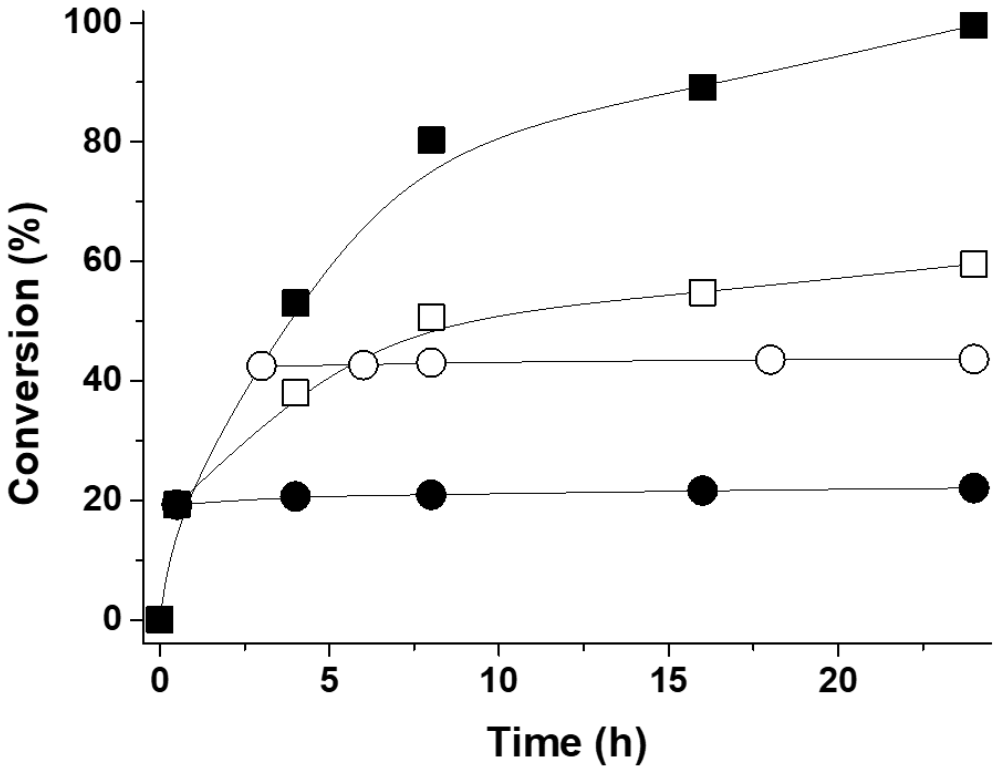

Figure 8. Time–conversion plots for the aerobic oxidation of cyclooctene to cyclooctene oxide using UiO-66($Zr_{5.4}$ $Ti_{0.6}$)-NO_2 as catalyst that is filtered at 0.5 h reaction time or that remains in contact with the substrate for the full reaction time. Legend: UiO-66($Zr_{5.4}$ $Ti_{0.6}$)-NO_2 (■), after catalyst filtration at 0.5 h (□), after catalyst filtration at 0.5 h and 20 mol% of TEMPO were added (●) and after catalyst filtration at 3h and 20 mol% of TEMPO were added(○). Reactions conditions: Catalyst (0.016 mmol of metal), substrate (2 mmol), CH_3CN (2 mL), 120 ºC and O_2 (5 atm).

To address the origin of the progress of cyclooctene oxidation in the hot filtration test, analysis of the Zr and Ti content in the liquid phase after filtration of the catalyst at 0,5 h in hot was performed. The results show that there was a negligible amount of Zr and Ti equivalent of 0.5% of the metal content present in the catalyst. It should be commented, however, that although the leached Zr and Ti metals was very small, there are precedents in the literature in where it has been found that small amounts of transition metals in the ppm range are sufficient to accelerate autooxidation reactions in a measurable extent.[57] Therefore, some contribution of these leached metal species cannot be totally disregarded.

To address this possible contribution of leached Zr and Ti species, we performed the previously commented control experiments shown in Figure 7 in where aerobic oxidation of cyclooctene was promoted using ZrO_2 and TiO_2, both at the concentration determined in the leaching analysis and at the concentration corresponding to the total amount of Zr and Ti present in UiO-66($Zr_{5.4}$ $Ti_{0.6}$)-NO_2. In both cases it was observed that although particularly TiO_2 exhibits some catalytic activity, it was much lower than that of UiO-66($Zr_{5.4}$ $Ti_{0.6}$)-NO_2. These catalytic experiments suggest some minor activity due to the leached Zr and Ti species, but far from that measured for UiO-66($Zr_{5.4}$ $Ti_{0.6}$)-NO_2. On the other hand, it is also known that autoxidation occurs through a chain

mechanism, in where chain propagation may result in the formation of a large number of product molecules with just a single initiation event.[57] Normally, the length of this propagation cycle is not relatively long when radicals are generated in cages and porous materials due to restrictions to the diffusion of these reaction intermediates.[57] However, when the catalyst is filtered, these free radicals present in the liquid phase could exhibit a much longer propagation chain length and in that way, they could contribute to the conversion of cyclooctene. In the related precedents in the literature, it was also observed that hot filtration does not stop aerobic oxidations of benzylic hydrocarbons and the role of the solid material was proposed to be more as solid initiator of carbon-centred radicals than a real catalyst in where active centers present in the solid carry out every turnover converting one substrate molecule into a product in each of them. Similarly here, it seems that, although not completely, UiO-66($Zr_{5.4}Ti_{0.6}$)-NO_2 could behave partially as solid initiator.[28] In the present case of UiO-66($Zr_{5.4}Ti_{0.6}$)-NO_2 a higher contribution about 65 % of the total conversion appears to correspond to a true catalyst.

To provide some evidence on the nature of the reaction intermediates responsible for the progress of cyclooctene oxidation in the hot filtration test after removal of the solid catalyst, 2,2,6,6-Tetramethylpiperidine 1-oxyl (TEMPO) was used as a quencher. It is well-known in the literature that TEMPO reacts with carbon center radicals trapping them and stopping the reaction.[57] Quenching experiments by TEMPO were carried out with 20 mol% of this quencher respect to cyclooctene. It was observed that addition of TEMPO in the clear solution after removal of the reaction completely stops further cyclooctene conversion under the reaction conditions (Figure 8). Moreover, if after the hot filtration test at 20% conversion TEMPO is added when conversion was 42 % at 4.5 hours, then, progress of cyclooctene conversion immediately stops at this point. These experiments with TEMPO conclusively demonstrate that carbon center radicals derived from

cyclooctene are the reaction intermediates responsible for the progress of the reaction after filtration of the solid catalyst and that these carbon center radicals do survive for hours in the reaction medium after filtration of the catalyst.

Reaction mechanism

To gain further insights into the reaction mechanism and, specifically, to obtain some evidence about the nature of the possible reactive oxygen species involved in the cyclooctene oxidation, quenching experiments using *p*-benzoquinone and DMSO were carried out. *p*-Benzoquinone is a selective quencher of hydroperoxide/superoxide,[54, 55, 57, 58] while DMSO quenches selectively hydroxyl radicals.[54-57] Thus, comparison of the performance of the cyclooctene oxidation in the absence and in the presence of quenchers (20 % molar proportion respect to substrate) could provide valuable information on the nature of the active oxygen species responsible for the reaction. The results of the quenching tests are presented in Figure 9. It should be noted that these quenchers are added at 0.5 h reaction time, when cyclooctene conversion was already about 20 % and possible intermediates have already been generated. Also, the amount of quencher was in substoichiometric ratio respect to the substrate. Figure 9 shows that the reaction stops almost completely upon addition of *p*-benzoquinone indicating that hydroperoxide/superoxide are likely to be involved in the process. More surprising was, however, the observation that DMSO, a selective hydroxyl radical quencher, also decreases significantly cyclooctene conversion, although it does not stop completely the reaction. Overall, the combined information of the kinetic data shown in Figure 9 can be understood considering that superoxide would be the primary oxygen radical species, and therefore, would be involved somehow in the formation of all the reaction product. In addition, more aggressive hydroxyl radicals should also be involved, but these hydroxyl radicals should not be the only reactive oxygen species because they do not account for

the whole product formation. Moreover, they would be formed as secondary intermediates from superoxide. Figure 9b proposes several pathways in which hydroxyl radicals could be generated. Accordingly, it seems that the main role of solid UiO-66($Zr_{5.4}$ $Ti_{0.6}$)-NO_2 solid material is to open additional pathways for oxygen activation and generation of reactive oxygen species (Figure 9b). EPR measurements using the UiO-66($Zr_{5.4}Ti_{0.6}$)-NO_2 as solid catalyst confirm the formation of hydroperoxy radicals by detecting its adduct with PBN-OOH (Figure 9d).[71-73]

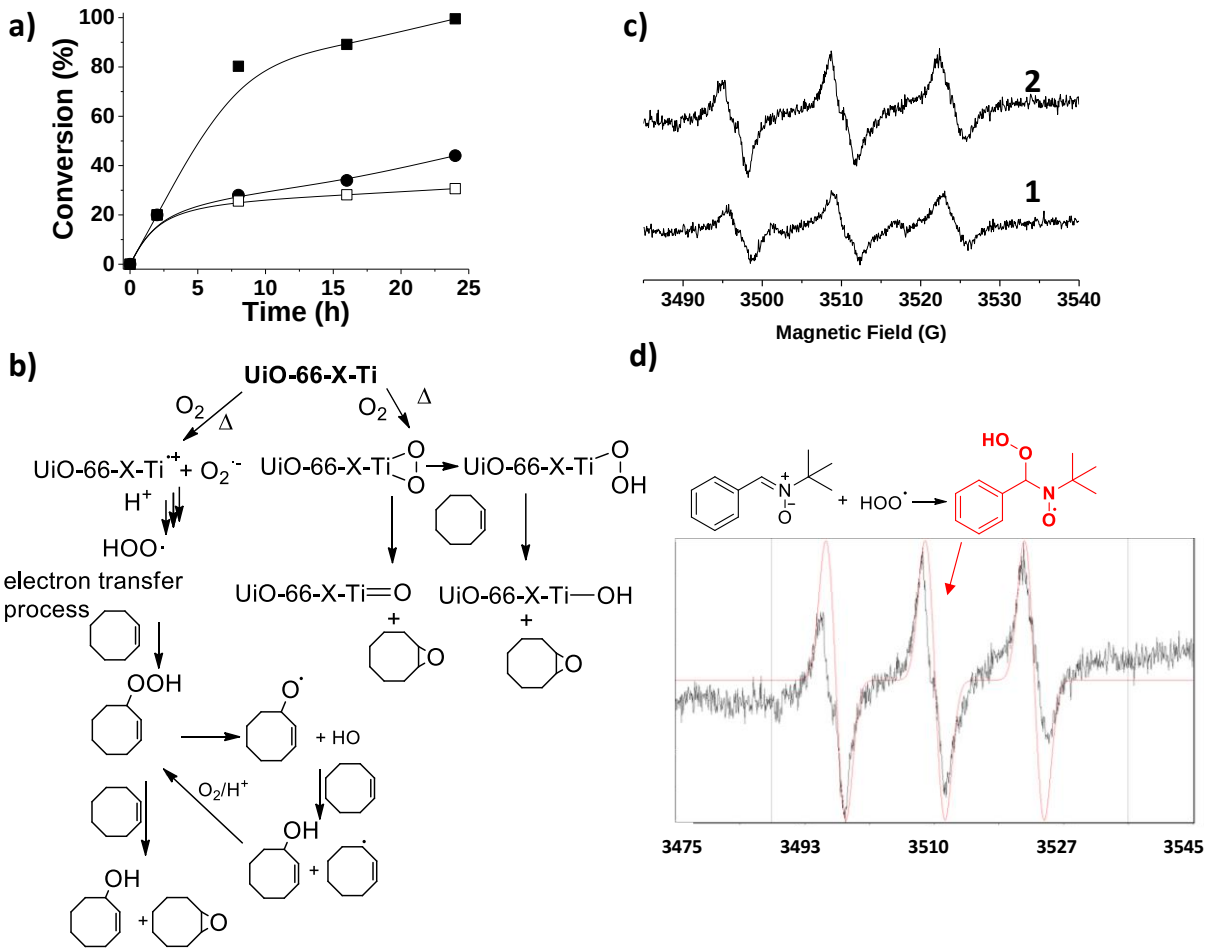

Figure 9. a) Time–conversion plots for the aerobic oxidation of cyclooctene to cyclooctene oxide using UiO-66($Zr_{5.4}$ $Ti_{0.6}$)-NO_2 as catalyst. Legend: In the absence of any quencher (■), upon

addition of 20 % DMSO (●) and upon addition of 20 % *p*-benzoquinone (□). Reactions conditions: Catalyst (0.016 mmol of metal), substrate (2 mmol), CH_3CN (2 mL), 120 ºC and O_2 (5 atm), quencher addition was made at 20% cyclooctene conversion. b) Proposed pathways for oxygen activation in the alkene oxidation using UiO-66($Zr_{5.4}$ $Ti_{0.6}$)-NO_2 as catalyst. c) Experimental EPR spectra obtained by using PBN + O_2 (1) and UiO-66($Zr_{5.4}$ $Ti_{0.6}$)-NO_2+ PBN + O_2 using *n*-dodecane as solvent at 120 ºC for 4 h. (d) Experimental (black) and simulated (red) EPR spectra of PBN-OOH adduct when using UiO-66($Zr_{5.4}$ $Ti_{0.6}$)-NO_2+ PBN + O_2 using *n*-dodecane as solvent at 120 ºC for 4 h. Experimental hyperfine coupling constants of PBN-OOH coinciding with those reported in literature AG_N = 14.0 and AG_H = 2.05.[28, 58, 74]

The role of molecular O_2 in the resulting catalytic activity was further confirmed by observing a linear relationship between the oxygen pressure and the initial reaction rate for cyclooctene epoxidation (Figure 10 a). This observation is in agreement with the proposed radical mechanism in which molecular O_2 reacts with carbon center radicals to form hydroperoxyl radicals as the rate determining step when using UiO-66($Zr_{5.4}$ $Ti_{0.6}$)-NO_2 as catalyst. The apparent activation energy for the aerobic cyclooctene oxidation was estimated by performing a series of reactions in the range of temperature between 110 and 140 ºC (Figure 10 b). From the Arrhenius plot of the natural logarithm of the initial reaction rate (r_0) against the inverse of the absolute temperature a value for the apparent activation energy of 36 $kJmol^{-1}$ was determined. This value is similar, but somewhat lower, to other activation energy values for aerobic oxidation of aromatic hydrocarbons using MOFs as catalysts or promoters.[57]

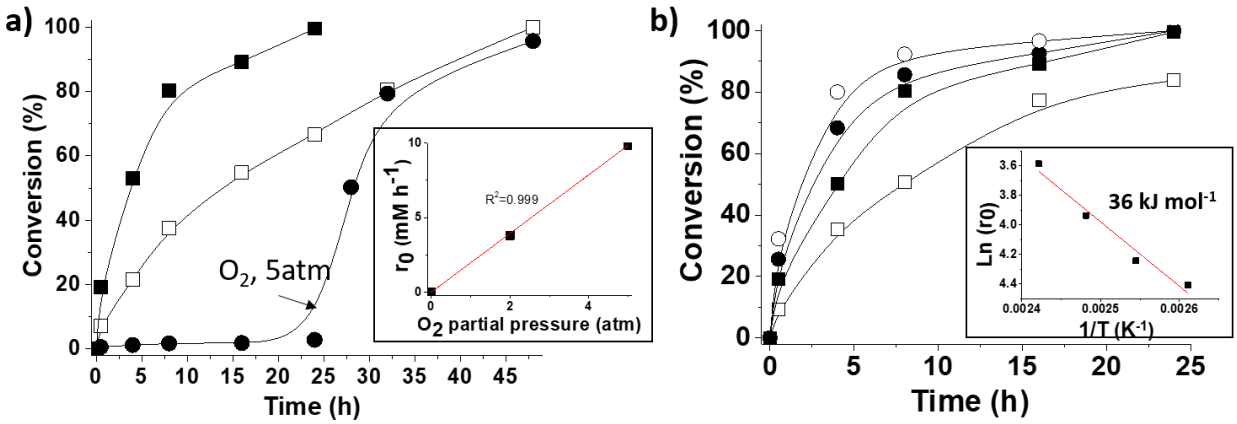

Figure 10. a) Influence of the oxygen partial pressure on the resulting catalytic activity of UiO-66($Zr_{5.4}$ $Ti_{0.6}$)-NO_2 for cyclooctene oxidation. The inset shows the linear relationship between the initial reaction rates of cyclooctene oxidation versus the oxygen partial pressure. Legend: oxygen (■), air (□), argon for 25 h and after 25 h oxygen (●). b) Time–conversion plots for the aerobic oxidation of cyclooctene to cyclooctene oxide using UiO-66($Zr_{5.4}$ $Ti_{0.6}$)-NO_2 as catalyst carried out at four different temperatures. The inset shows the Arrhenius plot for the aerobic oxidation cyclooctene to cyclooctene oxide based on the initial reaction rates r_0 obtained from the time–conversion plot. Legend: 110 °C (□), 120 °C (■), 130 °C (●), 140 °C (○). Reactions conditions: Catalyst (0.016 mmol of metal), substrate (2 mmol), CH_3CN (2 mL) and O_2 (5 atm).

One additional point of interest was to stablish weather or not the linker place any role in the generation of reactive oxygen species, for instance, by forming some organic peroxides. Aimed at the detection of organic peroxides for the linker, an additional experiment in which UiO-66($Zr_{5.4}$,$Ti_{0.6}$)-H was submitted to the reaction conditions at 120 ºC and 5 atm oxygen pressure in acetonitrile in the absence of any substrate was performed. These conditions were considered adequate to form peroxides of the organic linker because they are similar to the reaction conditions except that no cyclooctene is present. After 24 hours treatment the heated UiO-66($Zr_{5.4}$,$Ti_{0.6}$)-H

sample was submitted to the test to detect peroxides (see experimental section), but no evidence of the formation of these species could be obtained the failor to detect organic peroxides in UiO-66($Zr_{5.4}$,$Ti_{0.6}$)-H is in agreement with the reluctance of electron pore aromatics to form peroxides.

As commented before, the catalytic activity of UiO-66(Zr)-Ti increases both upon partial replacement of Zr^{4+} ions by Ti^{4+} atoms and by the presence of NO_2 on the terephthalate organic ligand. The most active catalyst for the aerobic oxidation of olefins is the UiO-66($Zr_{5.4}Ti_{0.6}$)-NO_2 material (Figure 5 a). In the introduction section it has been already indicated that isolated Ti^{4+} ions in a zeolitic framework have been previously reported to be active to promote oxidation reactions acting as Lewis acid.[39, 41] We speculate that the Lewis acidity of the parent UiO-66($Zr_{5.4}Ti_{0.6}$)-H solid should increase or decrease due to the presence of electron withdrawing or donor groups such as NO_2 or NH_2, respectively.[29] In fact, a linear relationship between the meta Hammett constant (σ_m) and the logarithm of r_0 was found (Figure 11 b).[30] To gain insight about the influence of NO_2 substitution on the acidity, an *in situ* FT-IR CO adsorption study on the series of UiO-66(Zr Ti)-X materials was carried out. It was observed that, the partial substitution of Zr by Ti atoms in the UiO-66($Zr_{5.4}$ $Ti_{0.6}$)-NO_2 material does not change the wavenumber of the Zr^{4+}-CO interaction. This fact is not unexpected considering the similar Lewis acidity of Zr^{4+} and Ti^{4+} ions. On the other hand, the presence of electron donor or withdrawing groups such as NH_2 or NO_2, respectively, causes a notable shift of the metal-CO frequency to lower or higher values, respectively. This observation correlates well with the proposed decrease or increase of the Lewis acidity of the UiO-66(ZrTi) material when bearing $–NH_2$ or NO_2 groups, respectively. We speculate that an increase in the Lewis acidity is beneficial for $HOO^{\cdot}$ activation, once formed from molecular O_2 and, then, epoxidation rates increases due to the higher polarization of the peroxy O-O bond.[39, 75]

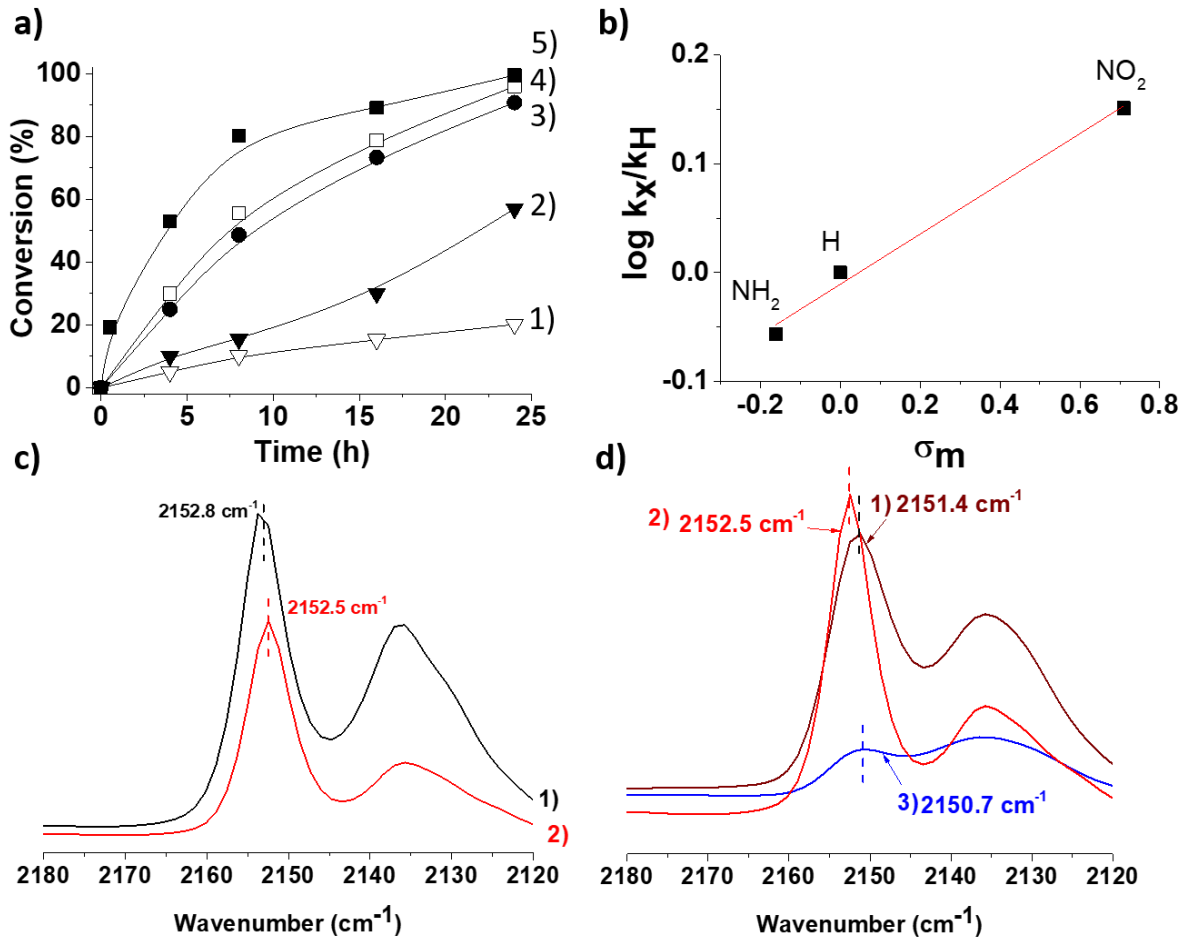

Figure 11. a) Time-conversion plots for cyclooctene epoxidation by O_2 catalyzed by a series of UiO-66(Zr/Ti)-X catalysts. Legend: absence of catalyst (1), UiO-66(Zr)-NO_2 (2), UiO-66($Zr_{5.4}$ $Ti_{0.6}$)-NH_2 (3), UiO-66($Zr_{5.4}$ $Ti_{0.6}$)-H (4) and UiO-66($Zr_{5.4}$ $Ti_{0.6}$)-NO_2 (5). Reaction conditions: Catalyst (0.016 mmol of metal of Zr+Ti), substrate (2 mmol), CH_3CN (2 mL), 120 ºC and O_2 (5 atm); b) Plot of the logarithm of the relative rate constants as a function of the meta Hammett constant (σ_m) of the substituent present on the terephthalate linker; c) FTIR spectra of CO adsorption at 6 mbar and -176 ºC on UiO-66(Zr)-NO_2 (1) and UiO-66($Zr_{5.4}$ $Ti_{0.6}$)-NO_2 (2). d) FTIR spectra of CO adsorption at 6 mbar and -176 ºC on UiO-66($Zr_{5.4}$ $Ti_{0.6}$)-H (1) and UiO-66($Zr_{5.4}$ $Ti_{0.6}$)-NO_2 (2) and UiO-66($Zr_{5.4}$ $Ti_{0.6}$)-NH_2 (3).

Scope of the catalyst

The present study about the aerobic oxidation of cyclooctene was expanded to determine the scope of UiO-66($Zr_{5.4}$ $Ti_{0.6}$)-NO_2 as catalyst. It is known in the literature that the size of the cycloalkene ring has a strong influence on the product distribution and, particularly, on the ratio between C=C epoxidation versus allylic oxidation that decreases from cyclooctene as the size of the ring decreases.[54, 55, 76] A similar trend was observed herein (Figure 12). Thus, while for cyclooctene the corresponding epoxide was the only product observed with almost complete selectivity, in the case of cycloheptene formation of the corresponding oxide was accompanied by formation of 2-cycloheptenone with a selectivity that changes as a function of the conversion Figure 12 shows the corresponding time-conversion and conversion-selectivity plots for cycloheptene oxidation using UiO-66($Zr_{5.4}$ $Ti_{0.6}$)-NO_2 as catalyst. As expected, in the case of cyclohexene, selectivity towards cyclohexene oxide was very low, being the allylic oxidation towards the corresponding ol/one mixture the major process with a selectivity value at final reaction time about 85 %. (Figure 12). One specific feature of cyclohexene is the shorter chain length of the propagation step in the autooxidation process compared to the case of cyclooctene. This is reflected by the fact that the hot filtration test for cyclohexene results upon removal of the solid UiO-66($Zr_{5.4}$ $Ti_{0.6}$)-NO_2, in a much lower progress of the conversion (15 %) as compared to the case of cyclooctene (35 %). Also, due to the shorter chain length and low concentration of active species outside the solid, in the case of cyclohexene, quenching experiments by *p*-benzoquinone and DMSO did not were positive, meaning that the reaction of cyclohexene takes place predominantly inside the porous of UiO-66($Zr_{5.4}$ $Ti_{0.6}$)-NO_2 near the active sites. The contribution due to free-radical oxidation outside the pores of UiO-66($Zr_{5.4}$ $Ti_{0.6}$)-NO_2 in the solution accounting for the 15% observed in the hot filtration test (Figure 12).

To confirm that both in the case of cyclooctene and cyclohexene epoxidation occurs through carbon center radical and that the difference in the percentage of progress of substrate conversion is due to the different radical chain length, after hot filtration of the catalyst TEMPO (20 mol%) was added to the clear solution in the absence of solid catalyst and the mixture was allowed to react in the reaction conditions. No further progress of cyclooctene and cyclohexene conversion was observed in the experiments were TEMPO as carbon radical quencher was present in comparison to the hot filtration test in the absence of TEMPO. Therefore, the different progress of cyclohexene and cyclooctene after filtration of the catalyst in the hot filtration test have to be attributed to the differences in the relative length on the propagation steps of the radical chain mechanism(Figure 8 and 12).

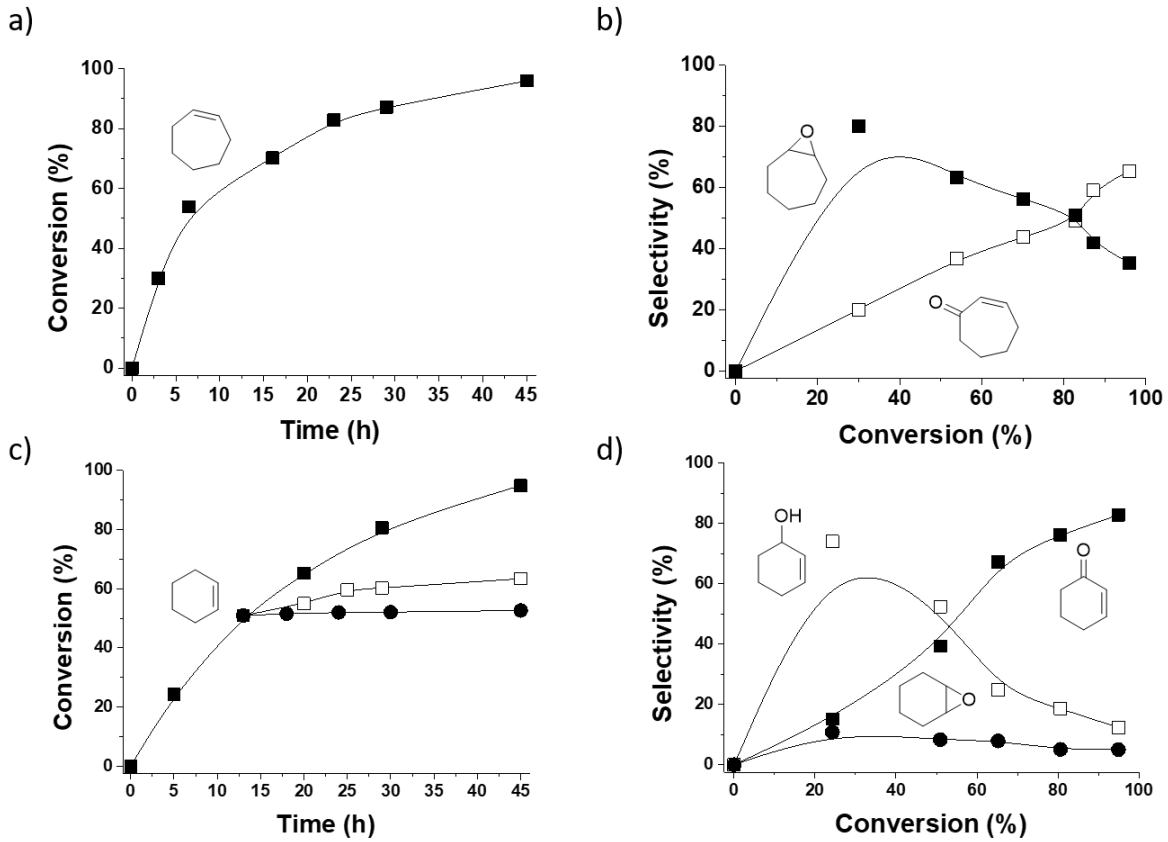

Figure 12. Time–conversion plots for the aerobic oxidation of cycloheptene (a) or cyclohexene (c) using UiO-66($Zr_{5.4}$ $Ti_{0.6}$)-NO_2 as catalyst. Selectivity-conversion plots for the aerobic oxidation of cycloheptene (b) or cyclohexene (d) to the corresponding reaction products as indicated in the plots. Legend c: UiO-66($Zr_{5.4}$ $Ti_{0.6}$)- NO_2 (■), after catalyst filtration at 13 h. (□) and after catalyst filtration at 13 h and 20 mol% of TEMPO were added (●). Reactions conditions: Catalyst (0.016 mmol of metal), substrate (2 mmol), CH_3CN (2 mL), O_2 (5 atm) and 120 ºC.

UiO-66($Zr_{5.4}$ $Ti_{0.6}$)-NO_2 was also able to promote the aerobic epoxidation of linear terminal alkenes such as 1-octene. In this case, kinetics is slower than for the cyclic analogues. This can be easily rationalized considering that diffusion of linear alkenes in porous materials is always slower than for the corresponding cyclic analogues and/or alternatively, the intrinsic activity of mono substituted terminal alkenes is lower than that of disubstituted cyclic compounds. What is remarkable in any case is the high selectivity of the UiO-66($Zr_{5.4}$ $Ti_{0.6}$)-NO_2 catalyst for the aerobic epoxidation that results in almost complete selectivity towards 1-octene oxide as it can be seen in Figure S29.

The scope of UiO-66(Zr Ti)-X as promoter of the aerobic oxidation of alkenes was expanded to aryl conjugated alkenes by studying the reaction of styrene and stilbene. In the case of styrene, oxidation gives rise to a mixture in which the product selectivity changes with conversion, the major product at final conversion being benzaldehyde with a selectivity of 40 %, accompanied by phenylacetaldehyde (15 %), acetophenone (15 %) and lesser amounts of styrene oxide (8 %) and benzoic acid (8 %) (Figure S30). Formation of all these products can be easily explained as derived from two competitive pathways. On one hand, the oxidative C=C bond cleavage results initially in benzaldehyde that subsequently undergoes further oxidation to benzoic acid. The second

pathway is epoxidation forming initially styrene oxide that undergoes rearrangement to the terminal (phenylacetaldehyde) or internal (acetophenone) carbonylic isomer.

In the case of *trans*-stilbene analogous two competitive pathways should take place leading to benzaldehyde (C=C bond cleavage) in lower selectivity (25 % at final reaction time) and trans-stilbene oxide (C=C epoxidation) that was the major product at final reaction time with 75 % of selectivity (Figure S31). Interestingly *cis*-stilbene was inert under these conditions and no oxidation products were observed in the presence of UiO-66($Zr_{5.4}$ $Ti_{0.6}$)-NO_2 under identical conditions. Again, this lack of reactivity of the *cis* isomer compared to the reactivity of *trans*-stilbene is a typical case of shape-selectivity catalysis.[77] It derives from the fact that the reaction in the case of conjugated alkenes takes place predominantly inside the pores where diffusion of *cis* isomer is impeded respect to the *trans*-stilbene due to the lower kinetic dimensions of the latter. These observations are in agreement with previous reports that have reported a smaller Lennard-Jones kinetic diameter for *trans*-stilbene (7.1 Å) compared with the bulkier *cis* isomer (7.8 Å).[78] Alternatively, the possibility that the *cis* isomer exhibits lower reactivity respect to the *trans* isomer cannot be ruled out. Thus, in contrast to the case of cyclooctene, where some degree of conversion occurs in the liquid phase, the lack of reactivity of *cis*-stilbene indicates that, for conjugated alkenes, the contribution of oxidation outside the pores should negligible. This observation is in accordance with basic knowledge in organic chemistry about the influence of chemical structure of organic compounds and their reactivity.

4. CONCLUSIONS

The present study has established that while UiO-66(Zr) is devoid of catalytic activity for oxygen activation, ion exchange of Zr^{4+} by Ti^{4+} introduces catalytic activity for aerobic oxidation of alkenes. The activity of Ti^{4+} containing UiO-66 can be further enhanced by introducing electron withdrawing groups in the ligand. In that way, the initial reaction rate for the conversion of cyclooctene to the corresponding epoxide can be optimized for UiO-66($Zr_{5.4}$ $Ti_{0.6}$)-NO_2 compared to the inactive parent UiO-66(Zr)-H, reaching TON values that are higher than those of the most active homogeneous catalysts. The most active sample of the series is also able to promote epoxidation of other cycloalkenes as well as some linear and aromatic alkenes, following the pattern expected according to the structure-reactivity of the substrate. Overall, since MOFs are constituted by nodes and linkers, the present study illustrate the strategy to create active sites by ion exchange at both components should be simultaneously tuned to boost and optimize the catalytic activity of each MOF for a particular chemical reaction. It is proposed that this strategy of combining ligand substitution with post-synthetic modification of metal nodes should be general and it can be useful for many other catalytic reactions involving Lewis acid sites as well as redox mechanism.

ASSOCIATED CONTENT

The following files are available free of charge. Characterization data by PXRD, FT-IR, TGA, XPS and SEM. Catalytic activity of UiO-66 based materials.

AUTHOR INFORMATION

Corresponding Author

*Email: sernaol@doctor.upv.es (ORCID number: 0000-0001-8423-0759); hgarcia@qim.upv.es (ORCID number: 0000-0002-9664-493X).

Author Contributions

The manuscript was written through contributions of all authors. All authors have given approval to the final version of the manuscript.

Notes

The authors declare no competing financial interest.

ACKNOWLEDGMENTS

Financial support by the Spanish Ministry of Economy and Competitiveness (Severo Ochoa and CTQ2014-53292-R and CTQ2015-69563-CO2-14) is gratefully acknowledged. Generalidad Valenciana is also thanked for funding (Prometeo 2017/018). SN thanks financial support by the Fundación Ramón Areces (XVIII Concurso Nacional para la Adjudicación de Ayudas a la Investigación en Ciencias de la Vida y de la Materia, 2016).

ABBREVIATIONS

MOF, metal-organic framework; TON; turnover number;

REFERENCES

1. Ishii, Y.; Sakaguchi, S.; Iwahama, T., Innovation of Hydrocarbon Oxidation with Molecular Oxygen and Related Reactions. *Adv. Synth. Catal.* **2001,** *343*, 393-427.
2. Tomás, R. A. F.; Bordado, J. C. M.; Gomes, J. F. P., P-xylene oxidation to terephthalic acid: A literature review oriented toward process optimization and development *Chem. Rev.* **2013,** *113*, 7421-7469.
3. Punniyamurthy, T.; Velusamy, S.; Iqbal, J., Recent advances in transition metal catalyzed oxidation of organic substrates with molecular oxygen. *Chem. Rev.* **2005** *105*, 2329-2363
4. Allen, S. E.; Walvoord, R. R.; Padilla-Salinas, R.; Kozlowski, M. C., Aerobic copper-catalyzed organic reactions. *Chem. Rev.* **2013,** *113*, 6234-6458.
5. Dhakshinamoorthy, A.; Alvaro, M.; Garcia, H., Metal–organic frameworks as heterogeneous catalysts for oxidation reactions. *Catal. Sci. Technol.* **2011,** *1*, 856-867.
6. Cornell, C. N.; Sigman, M. S., Recent progress in Wacker oxidations: Moving toward molecular oxygen as the sole oxidant. *Inorg. Chem.* **2007,** *46*, 1903-1909
7. Dhakshinamoorthy, A.; Santiago-Portillo, A.; Concepcion, P.; Herance, J. R.; Navalon, S.; Alvaro, M.; Garcia, H., Room temperature silylation of alcohols catalyzed by metal organic frameworks. *Catal. Sci. Technol.* **2017,** *7*, 2445-2449.
8. Gunasekaran, N., Aerobic oxidation catalysis with air or molecular oxygen and ionic liquids. *Adv. Synth. Catal.* **2015,** *357*, 1990-2010.
9. Wendlandt, A. E.; Suess, A. M.; Stahl, S. S., Copper-catalyzed aerobic oxidative C-H functionalizations: Trends and mechanistic insights. *Angew. Chem. Int. Ed* **2011,** *50*, 11062-11087.
10. Devic, T.; Serre, C., High valence 3p and transition metal based MOFs. *Chem. Soc. Rev.* **2014,** *43*, 6097-6115.
11. Férey, G., Hybrid porous solids: Past, present, future. *Chem. Soc. Rev.* **2008,** *37*, 191-214.
12. Kitagawa, S.; Kitaura, R.; Noro, S.-I., *Angew. Chem., Int. Ed.* **2004,** *43*, 2334-2237.
13. Furukawa, H., Cordova, K.E., O'Keeffe, M., Yaghi, O.M., The chemistry and applications of metal-organic frameworks. *Science* **2013,** *341*, 1230444.
14. Chughtai, A. H.; Ahmad, N.; Younus, H. A.; Laypkov, A.; Verpoort, F., Metal-organic frameworks: Versatile heterogeneous catalysts for efficient catalytic organic transformations. *Chem. Soc. Rev.* **2015,** *44*, 6804-6849.
15. Corma, A.; Garcia, H.; Llabrés i Xamena, F. X., Engineering metal organic frameworks for heterogeneous catalysis. *Chem. Rev.* **2010,** *110*, 4606-4655.
16. Farrusseng, D.; Aguado, S.; Pinel, C., Metal-organic frameworks: Opportunities for catalysis. *Angew. Chem. Int. Ed.* **2009,** *48*, 7502-7513.
17. Gascon, J.; Corma, A.; Kapteijn, F.; Llabrés i Xamena, F. X., Metal organic framework catalysis: Quo vadis? *ACS Catal.* **2014,** *4*, 361-378.
18. Yoon, M.; Srirambalaji, R.; Kim, K., Homochiral Metal Organic Frameworks for Asymmetric Heterogeneous Catalysis. *Chem. Rev.* **2012,** *112*, 1196-1231.
19. Huang, Y.-B.; Liang, J.; Wang, X.-S.; Cao, R., Multifunctional metal-organic framework catalysts: Synergistic catalysis and tandem reactions. *Chem. Soc. Rev.* **2017,** *46*, 126-157.
20. Li, Y.; Wang, H.; Xie, L.; Liang, Y.; Hong, G.; Dai, H., MoS2 Nanoparticles Grown on Graphene: An Advanced Catalyst for the Hydrogen Evolution Reaction. J. Am. Chem. Soc. 2011, *133*, 7296-7299.
21. Rogge, S. M. J.; Bavykina, A.; Hajek, J.; Garcia, H.; Olivos-Suarez, A. I.; Sepúlveda-Escribano, A.; Vimont, A.; Clet, G.; Bazin, P.; Kapteijn, F.; Daturi, M.; Ramos-Fernandez, E. V.;

Llabrés i Xamena, F. X.; Van Speybroeck, V.; Gascon, J., Metal-organic and covalent organic frameworks as single-site catalysts. *Chem. Soc. Rev.* **2017,** *46*, 3134-3184.
22. Tu, J.; Zeng, X.; Xu, F.; Wu, X.; Tian, Y.; Hou, X.; Long, L., Microwave-induced fast incorporation of titanium into UiO-66 metal–organic frameworks for enhanced photocatalytic properties. *Chem. Commun.* **2017,** *53*, 3361-3364.
23. Zhu, L.; Liu, X.-Q.; Jiang, H.-L.; Sun, L.-B., Metal-Organic Frameworks for Heterogeneous Basic Catalysis. *Chem. Rev.* **2017,** *117*, 8129-8176.
24. Gómez-Pozuelo, G.; Cabello, C. P.; Opanasenko, M.; Horáček, M.; Čejka, J., Superior Activity of Isomorphously Substituted MOFs with MIL-100(M=Al, Cr, Fe, In, Sc, V) Structure in the Prins Reaction: Impact of Metal Type. *ChemPlusChem* **2017,** *82*.
25. Mitchell, L.; Williamson, P.; Ehrlichov, B.; Anderson, A. E.; Seymour, V. R.; Ashbrook, S. E.; Acerbi, N.; Daniels, L. M.; Walton, R. I.; Clarke, M. L.; Wright, P. A., Mixed-Metal MIL-100(Sc,M) (M=Al, Cr, Fe) for Lewis acid catalysis and tandem C-C Bond formation and alcohol oxidation *Chem. Eur. J.* **2014,** *20*, 17185-17197.
26. Sun, Q.; Liu, M.; Li, K.; Han, Y.; Zuo, Y.; Chai, F.; Song, C.; Zhang, G.; Guo, X., Synthesis of Fe/M (M = Mn, Co, Ni) bimetallic metal organic frameworks and their catalytic activity for phenol degradation under mild conditions. *Inorg. Chem. Front.* **2017,** *4*, 144-153.
27. Zou, R.; Li, P.-Z.; Zeng, Y.-F.; Liu, J.; Zhao, R.; Duan, H.; Luo, Z.; Wang, J.-G.; Zou, R.; Zhao, Y., Bimetallic metal-organic frameworks: Probing the Lewis acid site for CO2 conversion. *Small* **2016,** *12*, 2334-2343.
28. Santiago-Portillo, A.; Blandez, J. F.; Navalón, S.; Álvaro, M.; García, H., Influence of the organic linker substituent on the catalytic activity of MIL-101(Cr) for the oxidative coupling of benzylamines to imines *Catal. Sci. Technol.* **2017,** *7*, 1351-1362.
29. Santiago-Portillo, A.; Navalón, S.; Concepción, P.; Álvaro, M.; García, H., Influence of Terephthalic Acid Substituents on the Catalytic Activity of MIL-101(Cr) in Three Lewis Acid Catalyzed Reactions. *ChemCatChem* **2017,** *9*, 2506-2511.
30. Vermoortele, F.; Vandichel, M.; de Voorde, B. V.; Ameloot, R.; Waroquier, M.; Van Speybroeck, V.; De Vos, D. E., Electronic effects of linker substitution on Lewis acid catalysis with metal–organic frameworks. *Angew. Chem. Int. Ed.* **2012,** *51*, 4887-4890.
31. Herbst, A.; Khutia, A.; Janiak, C., Brønsted instead of Lewis acidity in functionalized MIL-101Cr MOFs for efficient heterogeneous (nano-MOF) catalysis in the condensation reaction of aldehydes with alcohols. *Inorg. Chem.* **2014,** *53*, 7319−7333.
32. Blandez, J. F.; Santiago-Portillo, A.; Navalon, S.; Gimenez-Marques, M.; Alvaro, M.; Horcajada, P.; Garcia, H., Influence of functionalization of terephthalate linker on the catalytic activity of UiO-66 for epoxide ring opening. *J. Mol. Catal. A Chem.* **2016,** *425*, 332-339.
33. Panchenko, V. N.; Matrosova, M. M.; Jeon, J.; Jun, J. W.; Timofeeva, M. N.; Jhung, S. H., Catalytic behavior of metal-organic frameworks in the Knoevenagel condensation reaction. *J. Catal.* **2014,** *316*, 251-259.
34. Cohen, S. M., Modifying MOFs: New chemistry, new materials. *Chem. Sci.* **2010,** *1*, 32-36.
35. Cohen, S. M., Postsynthetic methods for the functionalization of metal-organic frameworks. *Chem. Rev.* **2012,** *112*, 970-1000.
36. Tanabe, K. K.; Cohen, S. M., Postsynthetic modification of metal–organic frameworks—a progress report. *Chem. Soc. Rev.* **2011,** *40*, 498-519.

37. Sun, D.; Liu, W.; Qiu, M.; Zhang, Y.; Li, Z., Introduction of a mediator for enhancing photocatalytic performance via post-synthetic metal exchange in metal–organic frameworks (MOFs). *Chem.Commun.* **2015,** *51*, 2056--2059.
38. Lee, Y.; Kim, S.; Kang, J. K.; Cohen, S. M., Photocatalytic CO2 reduction by a mixed metal (Zr/Ti), mixed ligand metal–organic framework under visible light irradiation. *Chem.Commun.* **2015,** *51*, 5735--5738.
39. Corma, A.; García, H., Lewis acids as catalysts in oxidation reactions: From Homogeneous to heterogeneous systems. *Chem. Rev.* **2002,** *102*, 3837-3892.
40. De Baerdemaeker, T.; Steenackers, B.; De Vos, D., Ti-substituted zeolite Beta: A milestone in the design of large pore oxidation catalysts. *Chem. Commun.* **2013,** *49*, 7474-7476.
41. De Vos, D. E.; Sels, B. F.; Jacobs, P. A., Practical heterogeneous catalysts for epoxide production. *Adv. Synth. Catal.* **2003,** *345*, 457-473.
42. Ratnasamy, P.; Srinivas, D.; Knözinger, H., Active sites and reactive intermediates in titanium silicate molecular sieves. *Adv. Catal.* **2004,** *48*, 1-169.
43. Clerici, M. G.; Bellussi, G.; Romano, U., Synthesis of propylene oxide from propylene and hydrogen peroxide catalyzed by titanium silicalite. *J. Catal.* **1991,** *129*, 159-167.
44. Hutchings, G. J.; Lee, D. F.; Minihan, A. R., Epoxidation of allyl alcohol to glycidol using titanium silicalite TS-1: effect of the reaction conditions and catalyst acidity. *Catal. Lett.* **1996,** *39*, 83-90.
45. Diao, Z. Y.; Han, L. L.; Wang, Z. X.; Dong, C. C., The adsorption and dissociation of O2 on Cu low-index surfaces. *Phys. Chem. B.* **2005,** *109*, 5739-5745.
46. Saedi, Z.; Tangestaninejad, S.; Moghadam, M.; Mirkhani, V.; Mohammadpoor-Baltork, I., MIL-101 metal–organic framework: A highly efficient heterogeneous catalyst for oxidative cleavage of alkenes with H2O2. *Catal. Comm.* **2012,** *17*, 18-22.
47. Tantanak, D.; Vincent, M. A.; Hillier, I. H., Elucidation of the mechanism of alkene epoxidation by hydrogen peroxide catalysed by titanosilicates: a computational study. *Chem. Commun.* **1998,** *0*, 1031-1032.
48. Santaclara, J. G.; Olivos-Suarez, A. I.; Gonzalez-Nelson, A.; Osadchii, D.; Nasalevich, M. A.; van der Veen, M. A.; Kapteijn, F.; Sheveleva, A. M.; Veber, S. L.; Fedin, M. V.; Murray, A. T.; Hendon, C. H.; Walsh, A.; Gascon, J., Revisiting the incorporation of Ti(IV) in UiO-type metal−organic frameworks: Metal exchange versus grafting and their implications on photocatalysis. *Chem. Mater.* **2017,** *29*, 8963−8967.
49. Sun, D.; Liu, W.; Qiu, M.; Zhang, Y.; Li, Z., Introduction of a mediator for enhancing photocatalytic performance via post-synthetic metal exchange in metal–organic frameworks (MOFs), *Chem. Commun.* **2015,** *51*, 2056-2059.
50. Cavka, J. H.; Jakobsen, S.; Olsbye, U.; Guillou, N.; Lamberti, C.; Bordiga, S.; Lillerud, K. P., A new zirconium inorganic building brick forming metal organic frameworks with exceptional stability. *J. Am. Chem. Soc.* **2008,** *130*, 13850-13851.
51. Kandiah, M.; Nilsen, M. H.; Usseglio, S.; Jakobsen, S.; Olsbye, U.; Tilset, M.; Larabi, C.; Quadrelli, E. A.; Bonino, F.; Lillerud, K. P., Synthesis and stability of tagged UiO-66 Zr-MOFs. *Chem. Mater.* **2010,** *22*, 6632-6640.
52. Santiago Portillo, A.; Baldoví, H. G.; García Fernandez, M. T.; Navalón, S.; Atienzar, P.; Ferrer, B.; Alvaro, M.; Garcia, H.; Li, Z., Ti as mediator in the photoinduced electron transfer of mixed-metal NH2-UiO-66(Zr/Ti): Transient absorption spectroscopy study and application in photovoltaic cell. *J. Phys. Chem. C* **2017,** *121*, 7015-7024.

53. Sempere, D.; Navalon, S.; Dančíková, M.; Alvaro, M.; Garcia, H., Influence of pretreatments on commercial diamond nanoparticles on the photocatalytic activity of supported gold nanoparticles under natural Sunlight irradiation. *Appl. Catal. B-Environ* **2013,** *142-143*, 259-267.
54. Blandez, J. F.; Navalon, S.; Alvaro, M.; Garcia, H., N-Hydroxyphthalimide anchored on diamond nanoparticles as a selective heterogeneous metal-free oxidation catalyst of benzylic Hydrocarbons and cyclic Alkenes by Molecular O2. *ChemCatChem* **2018**, 10, 198-205.
55. Cancino, P.; Vega, A.; Santiago-Portillo, A.; Navalon, S.; Alvaro, M.; Aguirre, P.; Spodine, E.; García, H., A novel copperIJII)–lanthanumIJIII) metal organic framework as a selective catalyst for the aerobic oxidation of benzylic hydrocarbons and cycloalkenes *Catal. Sci. Technol.* **2016,** *6*, 3727-3736.

56. Espinosa, J. C.; Navalón, S.; Álvaro, M.; García, H., Reduced Graphene Oxide as a Metal-Free Catalyst for the Light-Assisted Fenton-Like Reaction*ChemCatChem* **2016,** *8*, 2642-2648.

57. Santiago-Portillo, A.; Navalon, S.; Cirujano, F.; Llabrés i Xamena, F.; Alvaro, M.; Garcia, H., MIL-101 as reusable solid catalyst for autooxidation of benzylic hydrocarbons in the absence of additional oxidizing reagent. *ACS Catal.* **2015,** *5*, 3216–3224.
58. Gómez-Paricio, A.; Santiago-Portillo, A.; Navalón, S.; Concepción, P.; Alvaro, M.; Garcia, H., MIL-101 promotes the efficient aerobic oxidative desulfurization of dibenzothiophenes. *Green Chem.* **2016**, 508-515.
59. Sellers, R. M., Spectrophotometric determination of hydrogen peroxide using potassium titanium(IV) oxalate. *Analyst* **1980,** *105*, 950-954.
60. Brozek, C. K.; Dinca, M., Cation exchange at the secondary building units of metal–organic frameworks. *Chem. Soc. Rev.* **2014,** *43*, 5456--5467.
61. Hajek, J.; Caratelli, C.; Demuynck, R.; De Wispelaere, K.; Vanduyfhuys, L.; Waroquier, M.; Van Speybreck, V., On the intrinsic dynamic nature of the rigid UiO-66 metal–organic framework. *Chem. Sci.* **2018,** *9*, 2723-2732.
62. Smith, S. J. D.; Ladewig, B. P.; Hill, A. J.; Lau, C. H.; Hill, M. R., Post-synthetic Ti exchanged UiO-66 metal-organic frameworks that deliver exceptional gas permeability in mixed matrix membranes. *Sci. Rep.* **2015,** *5*, 7823.
63. Fang, Z.; Bueken, B.; De Vos, D. E.; Fischer, R., Defect-engineered metal–organic frameworks *Angew. Chem. Int. Ed* **2015,** *54*, 7234-7254.
64. Shearer, G. C.; Chavan, S.; Bordiga, S.; Svelle, S.; Olsbye, U.; Lillerud, K. P., Defect engineering: Tuning the porosity and composition of the metal–organic framework UiO-66 via modulated synthesis. *Chem. Mater.* **2016,** *28*, 3749-3761.
65. Cavka, J. H.; Jakobsen, S.; Olsbye, U.; Guillou, N.; Lamberti, C.; Bordiga, S.; Lillerud, K. P., A new zirconium inorganic building brick forming metal organic frameworks with exceptional stability, *J. Am. Chem. Soc.* **2008,** *130*, 13850-13851.
66. Iwahama, T.; Yoshino Y.; Keitoku T.; Sakaguchi, S.; Y., I., Efficient oxidation of alcohols to carbonyl compounds with molecular oxygen catalyzed by N-hydroxyphthalimide combined with a Co species. *J. Org. Chem.* **2000,** *65*, 6502-6507.
67. Kandiah, M.; Nilsen, M. H.; Usseglio, S.; Jakobsen, S.; Olsbye, U.; Tilset, M.; Larabi, C.; Quadrelli, E. A.; Bonino, F.; Lillerud, K. P., Synthesis and stability of tagged UiO-66 Zr-MOFs, *Chem. Mater.* **2010,** *22*, 6632-6640.

68. Nishiyama, Y.; Nakagawa, Y.; Mizuno, N., High turnover numbers for the catalytic selective epoxidation of alkenes with 1 atm of molecular oxygen, Angew. Chem. Int. Ed. **2001**¸40¸3639-3641.
69. Yamazaki, S., An improved methyltrioxorhenium-catalyzed epoxidation of alkenes with hydrogen peroxide. *Org. Biomol. Chem.* **2007,** *5*, 2109-2113.
70. Morlanes, N.; Notestein, J. M., Kinetic study of cyclooctene epoxidation with aqueous hydrogen peroxide over silica-supported calixarene–Ta (V). Appl. Catal. A.-Gen. **2010,** *387* (1-2), 45-54.
71. Burkitt, M. J.; Mason, R. P., Direct evidence for in vivo hydroxyl-radical generation in experimental iron overload: An ESR spin-trapping investigation. *Proc. Natl. Acad. Sci. USA* **1991,** *88*, 8440-8444.
72. Janzen, E. G.; Hinton, R. D.; Kotake, Y., Substituent effect on the stability of the hydroxyl radical adduct of α-phenyl N-tert-butyl nitrone (PBN). *Tetrahedron Lett.* **1992,** *33*, 1257-1260.
73. Janzen, E. G.; Kotake, Y.; Randall D., H., Stabilities of hydroxyl radical spin adducts of PBN-type spin traps. *Free Radical Bio. Med.* **1992,** *12*, 169-173.
74. Buettner, G. R., Spin trapping: ESR parameters of spin adducts. *Free Radic Biol Med.* **1987,** *3*, 259-303.
75. Joergensen, K. A., Transition-metal-catalyzed epoxidations. *Chem. Rev.* **1989,** *89*, 431-458.
76. Dhakshinamoorthy, A.; Alvaro, M.; Garcia, H., Aerobic oxidation of cycloalkenes catalyzed by iron metal organic framework containing N-hydroxyphthalimide. *J. Catal.* **2012,** *289*, 259-265.
77. Hu, S.; Liu, D.; Wang, C.; Chen, Y.; Guo, Z.; Borgna, A.; Yang, Y., Liquid-phase epoxidation of trans-stilbene and cis-cyclooctene over vanadium-exchanged faujasite zeolite catalysts. *Appl. Catal. A.-Gen.* **2010,** *386*, 74-82.
78. Metin, O.; Alcan Alp, N.; Akbayrak, S.; Biçer, A.; Serdar Gültekin, M. S.; zkar, S.; Bozkaya, U., Dihydroxylation of olefins catalyzed by zeolite-confined osmium(0) nanoclusters: an efficient and reusable method for the preparation of 1,2-cis-diols. *Green Chem.* **2012,** *14*, 1488-1492.